The Plant Cell, Vol. 32: 2178–2195, July 2020, www.plantcell.org © 2020 ASPB.

Dual Recognition of H3K4me3 and DNA by the ISWI Component ARID5 Regulates the Floral Transition in Arabidopsis

Lian-Mei Tan,[a,1] Rui Liu,[b,1] Bo-Wen Gu,[a] Cui-Jun Zhang,[a] Jinyan Luo,[c] Jing Guo,[a] Yuhua Wang,[c] Lixian Chen,[b,c,d] Xuan Du,[b] Sisi Li,[b] Chang-Rong Shao,[a] Yin-Na Su,[a] Xue-Wei Cai,[a] Rong-Nan Lin,[a] Lin Li,[a] She Chen,[a] Jiamu Du,[b,2] and Xin-Jian He[a,e,2]

[a] National Institute of Biological Sciences, Beijing 102206, China
[b] Institute of Plant and Food Science, Department of Biology, Southern University of Science and Technology, Shenzhen, Guangdong 518055, China
[c] National Key Laboratory of Plant Molecular Genetics and Shanghai Center for Plant Stress Biology, Chinese Academy of Sciences Center for Excellence in Molecular Plant Sciences, Chinese Academy of Sciences, Shanghai 201602, China
[d] University of Chinese Academy of Sciences, Beijing 100049, China
[e] Tsinghua Institute of Multidisciplinary Biomedical Research, Tsinghua University, Beijing 100084, China

ORCID IDs: 0000-0002-1445-4375 (L.-M.T.); 0000-0001-6805-7263 (R.L.); 0000-0003-2629-9963 (B.-W.G.); 0000-0002-3286-6912 (C.-J.Z.); 0000-0001-8349-1439 (J.L.); 0000-0003-1690-1746 (J.G.); 0000-0002-4497-0311 (Y.W.); 0000-0003-3261-9193 (L.C.); 0000-0001-9589-3566 (X.D.); 000-0002-7290-8128 (S.L.); 0000-0002-2098-9229 (C.-R.S.); 0000-0002-7319-5086 (Y.-N.S.); 0000-0001-8796-6374 (X.-W.C.); 0000-0003-4928-7279 (R.-N.L.); 0000-0001-6353-8594 (L.L.); 0000-0002-0830-3263 (S.C.); 0000-0002-1337-0786 (J.D.); 0000-0002-2878-7461 (X.-J.H.)

Chromatin remodeling and histone modifications are important for development and floral transition in plants. However, it is largely unknown whether and how these two epigenetic regulators coordinately regulate the important biological processes. Here, we identified three types of Imitation Switch (ISWI) chromatin-remodeling complexes in Arabidopsis (*Arabidopsis thaliana*). We found that AT-RICH INTERACTING DOMAIN5 (ARID5), a subunit of a plant-specific ISWI complex, can regulate development and floral transition. The ARID-PHD dual domain cassette of ARID5 recognizes both the H3K4me3 histone mark and AT-rich DNA. We determined the ternary complex structure of the ARID5 ARID-PHD cassette with an H3K4me3 peptide and an AT-containing DNA. The H3K4me3 peptide is combinatorially recognized by the PHD and ARID domains, while the DNA is specifically recognized by the ARID domain. Both PHD and ARID domains are necessary for the association of ARID5 with chromatin. The results suggest that the dual recognition of AT-rich DNA and H3K4me3 by the ARID5 ARID-PHD cassette may facilitate the association of the ISWI complex with specific chromatin regions to regulate development and floral transition.

INTRODUCTION

ATP-dependent chromatin-remodeling proteins regulate the packaging, unwrapping, and mobilization of nucleosomes and thereby affect DNA replication, DNA repair, and transcription (Narlikar, 2010; Toto et al., 2014). Imitation Switch (ISWI) is one of four families of ATP-dependent chromatin-remodeling proteins (ISWI, SWI/SNF, CHD, and INO80) in eukaryotes (Clapier and Cairns, 2009). By mediating nucleosome mobility, ISWI proteins regulate the appropriate spacing of nucleosomes within the genome (Gkikopoulos et al., 2011; Li et al., 2012). ISWI proteins typically associate with one to three accessory subunits and form multiple ISWI complexes in eukaryotes (Yadon and Tsukiyama, 2011; Bartholomew, 2014). Accessory subunits of the ISWI complexes either regulate nucleosome mobilization or facilitate the association of the ISWI complexes with specific chromatin sites (Toto et al., 2014). In Arabidopsis (*Arabidopsis thaliana*), there are two closely related ISWI chromatin-remodeling proteins, CHROMATIN-REMODELING PROTEIN11 (CHR11) and CHR17 (CHR11/17; Huanca-Mamani et al., 2005; Li et al., 2012; Smaczniak et al., 2012). Like ISWI chromatin remodelers in yeast (*Saccharomyces cerevisiae*) and metazoans, CHR11/17 are required for the even spacing of nucleosomes in the gene body (Li et al., 2014). Loss-of-function of CHR11/17 results in pleiotropic developmental defects and early flowering (Li et al., 2012; Smaczniak et al., 2012). To date, only the DDT-domain proteins RINGLET1 (RTL1) and RTL2 have been reported to be accessory subunits of ISWI complexes in Arabidopsis (Li et al., 2012; Dong et al., 2013). It remains to be determined whether the Arabidopsis ISWI complexes contain any other accessory subunits and how the accessory subunits function in the complexes.

Histone modifications are important epigenetic regulators that can mediate the association of chromatin-remodeling proteins with chromatin in a locus-specific manner. An ISWI complex was

[1] These authors contributed equally to this work.
[2] Address correspondence to dujm@sustech.edu.cn and hexinjian@nibs.ac.cn.
The author responsible for distribution of materials integral to the findings presented in this article in accordance with the policy described in the Instructions for Authors (www.plantcell.org) is: Xin-Jian He (hexinjian@nibs.ac.cn)
www.plantcell.org/cgi/doi/10.1105/tpc.19.00944

shown to associate with the histone modifications H3K4me3 and H4K16ac through its the DDT-domain–containing subunit BPTF in humans (Li et al., 2006; Wysocka et al., 2006; Ruthenburg et al., 2011). Because histone modifications function at the nucleosome level and co-exist with DNA, many regulators of histone modifications have direct or indirect DNA binding modules. In Arabidopsis, the histone H3K9 methyltransferases SUVH4, SUVH5, and SUVH6 can directly bind to methylated DNA by their SRA domains (Rajakumara et al., 2011; Du et al., 2014; Li et al., 2018). The histone H3K4me3 demethylase JUMONJI14 can bind to its target DNA sequence through the interactions with two NAC family transcription factors, NAC050 and NAC052 (Ning et al., 2015; Zhang et al., 2015). The histone H3K27me3 demethylase RELATIVE OF EARLY FLOWERING6 can directly bind to its target DNA sequence by its C-terminal zinc finger domains (Cui et al., 2016; Li et al., 2016a). Moreover, the DNA methyltransferases CHROMOMETHYLASE3 and CHROMOMETHYLASE2 can bind to H3K9me2 and thereby facilitate the coupling of DNA methylation with H3K9me2 (Du et al., 2012; Stroud et al., 2014). Although these studies demonstrate that crosstalk occurs between histone modifications and DNA, little is known about whether and how histone modifications and DNA are combinatorially recognized by the ISWI complexes.

In plants, the floral transition refers to the switch from vegetative growth to reproductive growth. Because the transition requires many gene regulatory events, it involves multiple genetic and epigenetic regulation pathways (Bäurle and Dean, 2006; Imaizumi and Kay, 2006; Amasino, 2010). Among them, histone modifications and chromatin remodeling play important roles (Li et al., 2007; Jarillo et al., 2009; Berr et al., 2011). Here, we identified three types of Arabidopsis ISWI chromatin remodeling complexes, which we named CHR11/17-RLT1/2-ARID5 (CRA), CHR11/17-DDP1/2/3-MSI3 (CDM), and CHR11/17-DDR1/3/4/5/DDW1 (CDD). We found that all components of the CRA complex are required for development and floral transition. AT-RICH INTERACTING DOMAIN5 (ARID5) contains an ARID-PHD cassette that can simultaneously recognize the H3K4me3 histone mark and AT-rich DNA. We determined the crystal structure of the ARID-PHD cassette in complex with both an H3K4me3 peptide and an AT dinucleotide-containing DNA. The H3K4me3 is specifically recognized by the PHD and ARID domains in a combinatorial way, while the AT-containing DNA is mainly recognized by the ARID domain. Our results reveal how a critical ISWI complex component binds to specific chromatin regions to regulate development and floral transition.

RESULTS

Identification of Multiple ISWI Complexes in Arabidopsis

To identify the components of Arabidopsis ISWI complexes, we generated transgenic plants expressing CHR11-Flag and CHR17-Flag fusion proteins and performed immunoprecipitation followed by mass spectrometry (IP-MS) to isolate their interaction proteins. The in vivo function of the *CHR11-Flag* transgene was confirmed by complementation testing (Supplemental Figure 1). With IP-MS, we identified a large amount of CHR11 and CHR17 proteins in *CHR11-Flag* and *CHR17-Flag* transgenic plants (Figure 1A; Supplemental Table 1; Supplemental Data Set 1). In addition, several DDT-domain proteins, including RLT1, RLT2, DDT-PHD PROTEIN1 (DDP1), DDP2, DDP3, DDT-RELATED PROTEIN1 (DDR1), DDR3, DDR4, DDR5, and DDT-WAC PROTEIN1 (DDW1), were co-purified with CHR11 and CHR17 (Figure 1A), which is consistent with previous reports that the DDT-domain proteins associate with CHR11 and CHR17 as determined by yeast two-hybrid (Y2H) assay (Li et al., 2012; Dong et al., 2013). We further identified that ARID5, an ARID-containing protein, and MSI3, a homolog of the mammalian Retinoblastoma-associated proteins 46 and 48, were co-purified with CHR11 and CHR17 (Figure 1A), suggesting that they may function as subunits of ISWI complexes in Arabidopsis.

Next, we selected genes encoding different classes (DDPs, DDRs, and DDW1) of DDT-domain proteins and generated transgenic plants expressing these genes tagged by Flag epitope. Using IP-MS, we found that CHR11 and CHR17 were co-purified from all of the transgenic plants (Figure 1A; Supplemental Data Set 1), suggesting that CHR11 and CHR17 associate with all of the DDT-domain proteins tested in the experiment. DDR1, DDR3, DDR4, DDR5, and DDW1 were co-purified with CHR11 and CHR17 but not with other proteins (Figure 1A), indicating that CHR11 and CHR17 form ISWI complexes with these proteins without the involvement of other subunits. We termed these ISWI complexes CHR11/17-DDR1/3/4/5/DDW1 (CDD).

Unlike DDRs and DDW1 that were only co-purified with CHR11 and CHR17, RLT1 and RLT2 were co-purified not only with CHR11/17 but also with ARID5, and DDP2 and DDP3 were co-purified not only with CHR11/17 but also with MSI3 (Figure 1A; Supplemental Table 1). We generated transgenic plants expressing Myc-tagged ARID5 and Flag-tagged MSI3 and detected co-purified proteins. As expected, we found that ARID5 was co-purified with CHR11, CHR17, RLT1, and RLT2, while MSI3 was co-purified with CHR11, CHR17, DDP1, and DDP2 (Figure 1A; Supplemental Table 1). Therefore, we identified two types of Arabidopsis ISWI complexes, which we named CHR11/17-RLT1/2-ARID5 (CRA) and CHR11/17-DDP1/2/3-MSI3 (CDM).

Given that ARID5 is conserved in plants but not in other eukaryotes (Supplemental Figure 2), the CRA-type of ISWI complex may represent a plant-specific type of ISWI complex. Considering that MSI3 is an ortholog of Retinoblastoma-associated proteins 46 and 48, which are conserved subunits of the NURF ISWI complex in mammals (Martínez-Balbas et al., 1998), we predicted that the Arabidopsis CDM-type of ISWI complex is related to the mammalian NURF-type of ISWI complexes. While the ISWI complex components can be identified by IP-MS from transgenic plants expressing ISWI complex components, none of the components can be identified from five independent negative controls (Col-0; Supplemental Data Set 1), strongly suggesting that the identification of the ISWI complexes by IP-MS is reliable.

Interactions of ISWI Components as Determined by Y2H Assays

We conducted Y2H assays to determine how CHR11/17, ARID5, MSI3, and DDT-domain proteins interact with each other.

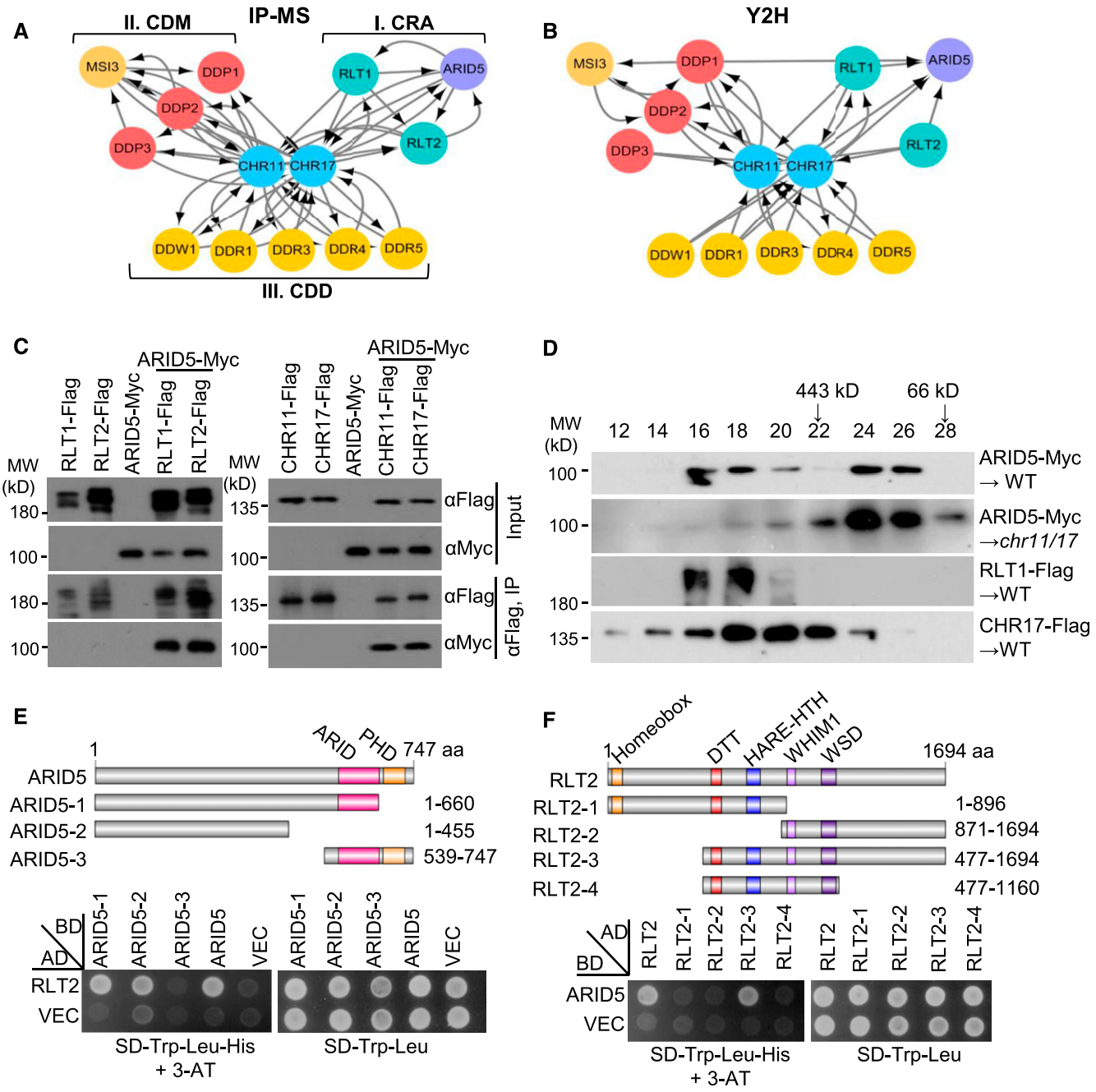

Figure 1. Identification and Characterization of ISWI Complexes in Arabidopsis.

(A) Protein–protein interaction network of subunits of multiple ISWI complexes as determined by IP-MS. Nodes denote ISWI subunits identified in this study; edges represent interactions between ISWI subunits. Arrows indicate that proteins were co-purified by affinity purification. Co-purified proteins are shown with arrowheads at the end of edges.

(B) Protein–protein interaction network of subunits of multiple ISWI complexes as determined by Y2H assays. A pair of nodes linked by double edges indicates that the interaction was verified bidirectionally by Y2H assay.

(C) Determination of the interaction of ARID5 with RLT1, RLT2, CHR11, and CHR17 by co-immunoprecipitation in corresponding transgenic plants.

(D) ARID5, RLT1/2, and CHR11/17 form large-molecular–weight complexes as determined by gel filtration. Proteins extracted from indicated epitope-tagged transgenic plants were separated in a Superose 6 column (10/300 GL; GE Healthcare Life Sciences) and were detected by immunoblotting.

(E) and **(F)** Identification of the ARID5- and RLT2-interaction domain using truncated ARID5 and RLT2 sequences by Y2H assays. Schematic representation of the ARID5 and RLT2 proteins and their truncated versions is shown in the top representation. The strains harboring the indicated constructs were grown on SD medium minus Trp and Leu, and on SD medium minus Trp, Leu, and His supplemented by 3 mM of 3-amino-1,2,4-triazol (3-AT).

Consistent with previous studies (Li et al., 2012; Dong et al., 2013), CHR11/17 interacted with all of the tested DDT-domain proteins (Figure 1B; Supplemental Figure 3; Supplemental Table 2). Moreover, ARID5 interacted with RLT1 and RLT2 but not with CHR11/17 (Figure 1B), even though ARID5 and CHR11/17 were co-purified with each other in Arabidopsis (Figure 1A). Given that RLT1/2 interacted with both ARID5 and CHR11/17 in the Y2H assay, we suspected that RLT1/2 may function as bridge proteins between ARID5 and CHR11/17 in the CRA-type of ISWI complex.

Unexpectedly, ARID5 also interacted with DDP1, DDR1, and DDW1 as determined by the Y2H (Figure 1B; Supplemental Figure 3; Supplemental Table 2). However, because ARID5 was not shown to associate with DDP1, DDR1, and DDW1 in Arabidopsis as determined by IP-MS (Figure 1A; Supplemental Table 1), the interaction of ARID5 with DDP1, DDR1, and DDW1 as determined by the Y2H is likely to be false positives. Alternatively, we cannot absolutely exclude the possibility that ARID5 may interact with DDP1, DDR1, and DDW1 in certain specific developmental stages or tissues.

The Y2H assay also indicated that MSI3 interacts with the DDT-domain proteins DDP1 and DDP2 (Figure 1B; Supplemental Figure 3; Supplemental Table 2). Like ARID5, MSI3 did not interact with CHR11/17 (Figure 1B), suggesting that the DDT-domain proteins may also function as bridge proteins between CHR11/17 and MSI3 in the CDM-type ISWI complex. Of note, not all pairwise interactions can be identified by both the AD/BD and BD/AD experiments (Figure 1B; Supplemental Figure 3; Supplemental Table 2**)**. This is caused by the technical limitation of Y2H. Because we tested the protein-protein interactions only when the interactions were primarily identified by IP-MS, the interactions detected by Y2H provide additional evidence to support the interactions that were identified by IP-MS.

Characterization of the CRA-Type ISWI Complex

Given that the CRA-type ISWI complex may be plant-specific, our further work mainly focused on the CRA-type ISWI complex. We generated transgenic plants expressing a native promoter-driven *ARID5* gene tagged by the *Myc* epitope (*ARID5-Myc*). The *ARID5-Myc* transgenic plants were crossed to the wild-type plants and to the transgenic plants expressing *CHR11-Flag*, *CHR17-Flag*, *RLT1-Flag*, and *RLT2-Flag* transgenes. Progeny plants expressing both the *ARID5-Myc* transgene and each of the *Flag*-tagged transgenes were subjected to co-IP. The results indicated that ARID5-Myc was co-precipitated with CHR11-Flag, CHR17-Flag, RLT1-Flag, and RLT2-Flag (Figure 1C), confirming that ARID5 interacts with CHR11, CHR17, RLT1, and RLT2.

We also performed gel filtration to determine the formation of the CRA-type ISWI complex in Arabidopsis. Proteins extracted from tagged transgenic plants were separated on a Superose 6 column (10/300 GL; GE Healthcare Life Sciences); the eluted fractions were detected by immunoblotting. The results indicated that ARID5, RLT1, and CHR17 were co-eluted in the fractions 16 to 18, which correspond to high molecular weights (Figure 1D). In the *chr11/17* mutant, however, the ARID5 signal was absent in the fractions 16 to 18 (Figure 1D). These results confirm that CHR11/17, RLT1/2, and ARID5 form large complexes.

Using Y2H assays with a series of truncated ARID5 and RLT2 sequences, we found that the full N-terminal region of ARID5 (ARID5-2, residues 1 to 455) and the RLT2 region containing DDT, HARE-H, WHI, and WSD domains (RLT2-3, residues 477 to 1,694) are responsible for the interaction between ARID5 and RLT2 (Figures 1E and 1F; Supplemental Figure 4). Furthermore, the interaction of RLT2 with both ARID5 and CHR11 was confirmed by an in vitro pull-down assay (Supplemental Figure 5), suggesting that RLT1/2 is responsible for recruiting ARID5 to the CRA-type ISWI complex.

The CRA Complex Regulates Development, Floral Transition, and Gene Expression

Defects in development and floral transition were previously reported in the *chr11 chr17* (*chr11/17*) double mutant and to a lesser extent in the *rlt1 rlt2* (*rlt1/2*) double mutant (Li et al., 2012). As compared with the wild-type plants, the *arid5* mutant plants were smaller and exhibited early flowering and decreased numbers of rosette leaves (Figures 2A to 2C). Moreover, the siliques of the *arid5* mutant were markedly shorter than the wild type (Supplemental Figure 6). The defects in the *arid5* mutant were similar to those in *rlt1/2* (Figures 2A and 2B; Supplemental Figure 6), which is consistent with the fact that both ARID5 and RLT1/2 are subunits of the CRA-type ISWI complex. A native promoter-driven *ARID5-Myc* transgene complemented the defects in *arid5* (Figure 2C). These results confirm that ARID5 functions as a subunit of the CRA-type ISWI complex to regulate development and floral transition.

To determine whether ARID5 co-regulates gene expression with RLT1/2 and CHR11/17 at the whole-genome level, we performed RNA deep sequencing (RNA-seq). A large number of genes were either up- or downregulated in the *arid5* (915 up and 558 down), *rlt1/2* (1,568 up and 1,092 down), and *chr11/17* (2,768 up and 2,688 down) mutants ($P < 0.01$; log2 (fold change) >1 or <−1, using the software Cufflinks (https://github.com/cole-trapnell-lab; Figure 2D; Supplemental Data Set 2). The pattern of differentially expressed genes (DEGs) in *arid5* is highly similar to that in *rlt1/2* and *chr11/17* (Figure 2E). Among DEGs in *chr11/17*, 39.5% (1,092/2,768) upregulated genes and 28.1% (754/2,688) downregulated genes were shared in *rlt1/2* (Figure 2D). The shared DEGs are likely to be regulated by the CRA-type ISWI complex, whereas the remaining DEGs in *chr11/17* may be regulated by the other types of ISWI complexes. Consistently, the DEGs in *arid5* significantly overlapped with the DEGs shared by *rlt1/2* and *chr11/17* but not with the remaining DEGs in the *chr11/17* mutant (Figure 2D).

Because *arid5*, *rlt1/2*, and *chr11/17* mutants affect the floral transition (Figures 2A and 2B), we investigated whether flowering-time genes are co-regulated in *arid5*, *rlt1/2*, and *chr11/17* as determined by RNA-seq. A previous study documented 306 flowering-time genes in Arabidopsis (Bouché et al., 2016). As shown by scatterplots (Figure 2F), the effect of *arid5* on the expression of the flowering-time genes is highly correlated with the effect of *rlt1/2* and *chr11/17*. In particular, the critical flowering-repressor genes *FLOWERING LOCUS C* (*FLC*) and *SHORT VEGETATIVE PHASE* (*SVP*) were co-downregulated in *chr11/17*, *rlt1/2*, and *arid5*, while the key flowering-promoter gene

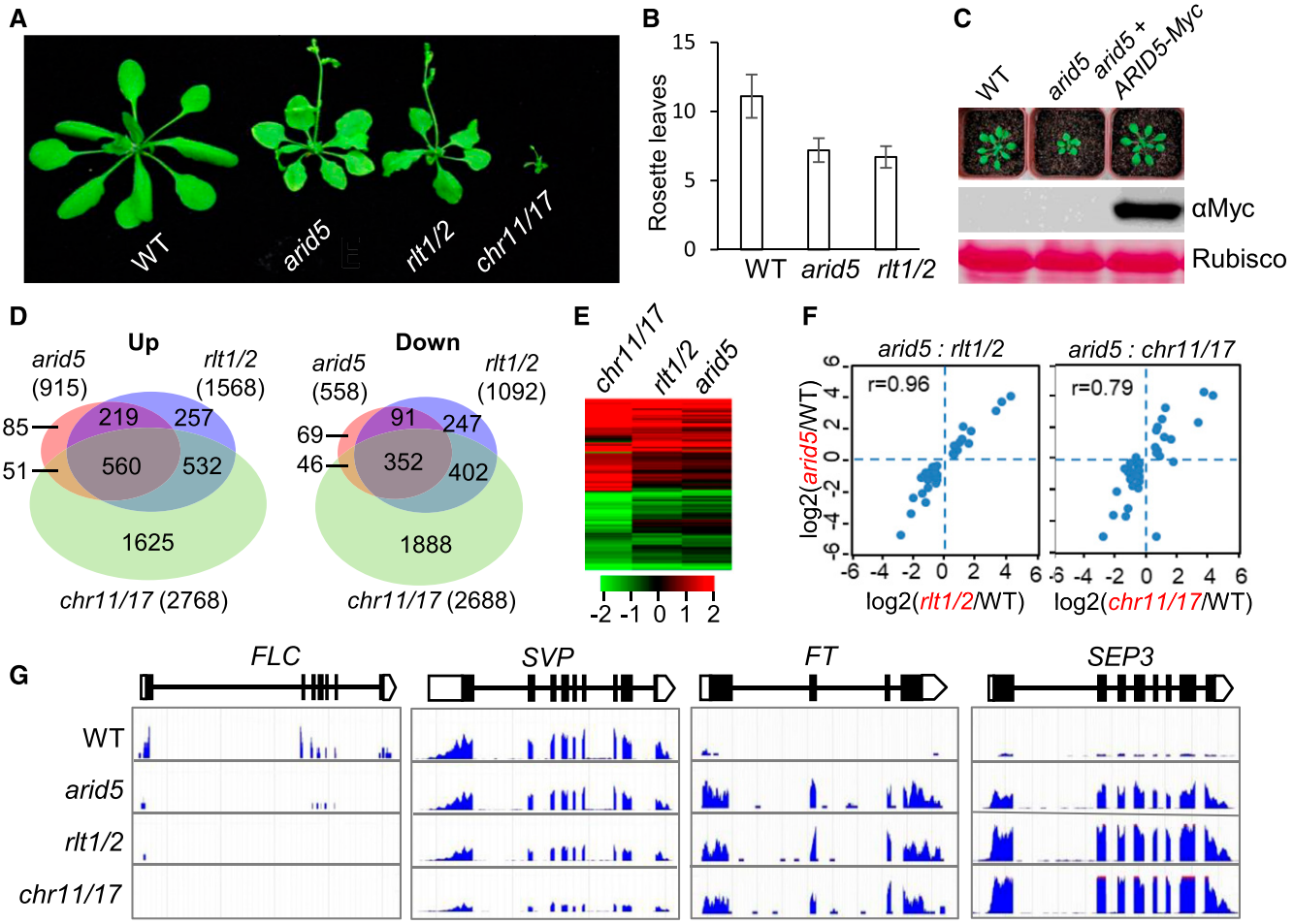

Figure 2. ARID5 Is Functionally Related to RLT1/2 and CHR11/17 in the Regulation of Development, Floral Transition, and Gene Expression.

(A) Morphological phenotypes of wild-type (WT), *arid5*, *rlt1/2*, and *chr11/17* mutant plants. Three-week–old plants of the indicated genotypes are shown.
(B) Effect of *arid5* and *rlt1/2* on flowering time. Flowering time was evaluated based on the number of rosette leaves when the plants began to bolt. Rosette leaves from at least 20 plants were counted.
(C) Morphologic phenotypes of the wild-type, *arid5*, and a representative *ARID5-Myc* transgenic line in the *arid5* mutant background. Two-week–old seedlings of the indicated genotypes are shown. The expression of the *ARID5-Myc* transgene was determined by immunoblotting. Ribulose-1,5-bis-phosphate carboxylase/oxygenase stained by Ponceau S was used as a loading control.
(D) Venn diagrams showing DEGs (relative to the wild type) identified by RNA-seq in the *arid5*, *rlt1/2*, and *chr11/17* mutants. RNA was extracted from 10-d–old seedlings.
(E) Heatmap of relative expression patterns of DEGs identified in the *arid5* mutant. Red and green represent up- and downregulated genes, respectively.
(F) Scatterplots showing the correlation of the expression changes of flowering-time genes between the *arid5* mutant and the *rlt1/2* mutant or the *chr11/17* mutant.
(G) Genome browser view of RNA-seq signals at *FLC*, *SVP*, *FT*, and *SEP3* in the wild type and in *arid5*, *rlt1/2*, and *chr11/17* mutants. Diagrams of genes are shown in the top representation. Blank boxes, filled boxes, and lines represent untranslated regions, coding regions, and introns, respectively.

FLOWERING LOCUS T (*FT*) and the floral identity gene *SEPALLATA3* (*SEP3*) were co-upregulated (Figure 2G; Supplemental Figure 7). Therefore, ARID5, RLT1/2, and CHR11/17 co-regulate the expression of the flowering-time genes and thereby control the floral transition.

To determine whether ARID5, RLT1/2, and CHR11/17 regulate the expression of genes involved in other biological processes, we conducted gene-ontology analysis for the DEGs co-regulated in the *arid5*, *rlt1/2*, and *chr11/17* mutants and found that the DEGs are enriched in genes related to abscission, defense response, and response to toxic substance (Supplemental Figure 8), suggesting that the CRA-type ISWI complex is involved not only in the regulation of flowering time but also in multiple other biological processes.

ARID5 Binds To Both DNA and H3K4me3 Functionally

ARID5 contains not only an ARID domain but also a PHD finger in the C-terminal region (Figure 3A). The PHD finger has been extensively reported to be a reader module for methylated or

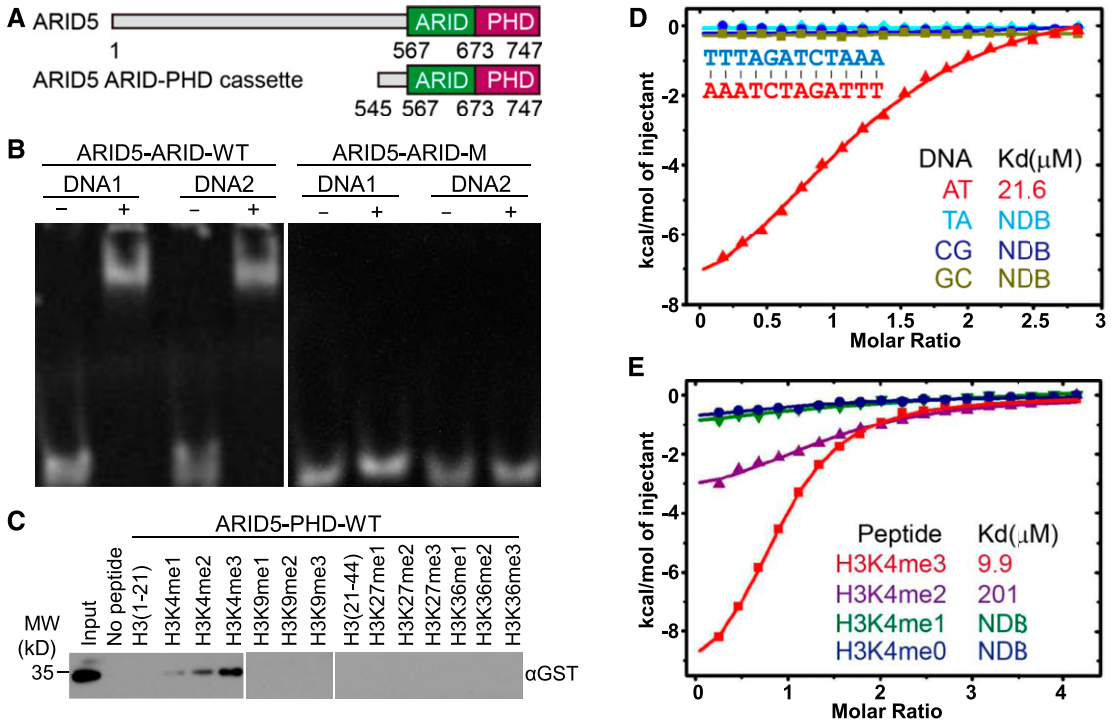

Figure 3. The ARID5 ARID-PHD Cassette Interacts with Both the H3K4me3 Histone Mark and AT-Containing DNA.

(A) A schematic representation of the domain architecture of Arabidopsis ARID5 (upper representation) and the construct used for biochemical studies (lower representation).

(B) An EMSA experiment showing that the ARID5 ARID domain can bind to AT-containing DNA. The AT-containing DNA1 and DNA2 are from the genic regions of *FLC* and the sequences are indicated in Supplemental Data Set 4.

(C) The specific binding of the ARID5 PHD domain to methylated H3K4 as determined by histone peptide pull-down assays.

(D) The ITC measurement of the binding affinity between the ARID5 ARID-PHD cassette and an AT-containing DNA as well as DNA duplexes in which the central AT di-nucleotides were replaced with TA, CG, and GC. The AT-containing DNA sequence used for measurement of ITC binding and crystallization is shown.

(E) ITC binding experiments showing that the ARID5 ARID-PHD cassette binds to methylated H3K4 with a preference for the H3K4me3.

unmethylated histone marks (Li and Li, 2012), and the ARID domain always functions in recognition of AT-rich DNA (Wilsker et al., 2002). To test the histone and DNA binding properties of ARID5, we performed biochemical binding assays. Our electrophoretic mobility shift assay (EMSA) showed that the expressed ARID5 ARID domain can efficiently interact with the AT-containing DNA probe (Figure 3B). Our in vitro pull-down assays indicated that the ARID5 PHD domain binds to the histone H3 peptide methylated at K4 but not at K9, K27, or K36 (Figure 3C). Next, we expressed the ARID-PHD dual domain cassette and measured the binding affinity of the cassette with a 12-bp central AT-containing DNA and an H3K4me3 peptide by isothermal titration calorimetry (ITC) assays. The results indicated that the binding affinity of the ARID-PHD cassette with the DNA and the peptide was measured to be 21.6 μM and 9.9 μM, respectively (Figures 3D and 3E). The binding affinity of the cassette with the H3K4me3 peptide is higher than with other lower-methylated states of H3K4 (Figure 3E).

To investigate whether the PHD and ARID cassette is required for the regulation of development and floral transition, we generated constructs expressing Myc-tagged PHD-deleted AIRD5 (ARID5-ΔPHD) and ARID-mutated ARID5 (ARID5-ARID-M; P598A/W630A) and transformed them into the *arid5* mutant for complementation testing. ARID5-ARID-M carried mutations in two conserved residues of the ARID domain and failed to bind to AT-containing DNA as determined by EMSA (Figure 3B). The *ARID5-WT* construct complemented the defects in development and floral transition of the *arid5* mutant, but the *ARID5-ΔPHD* and *ARID5-ARID-M* constructs did not complement or only weakly complemented the defects, even though their expression levels were comparable to the wild type (Figures 4A and 4B; Supplemental Figure 9). The expression of the flowering-time genes *FLC*, *SVP*, *FT*, and *SEP3* were either up- or down-regulated in the *arid5* mutant (Figure 2G). The ARID5-ΔPHD and ARID5-ARID-M transgenes either did not affect or only partially restored the expression of these genes in the *arid5* mutant, whereas the *ARID5-WT* transgene completely restored the expression of these genes (Figure 4C). We also generated *GFP*-tagged wild-type and mutated *ARID5* constructs for complementation testing. We found that, while the wild-type *ARID5-GFP* construct complemented the defects in development and floral transition of the *arid5* mutant, both the *ARID5-ΔPHD* and *ARID5-ARID-M* constructs failed to complement the defects

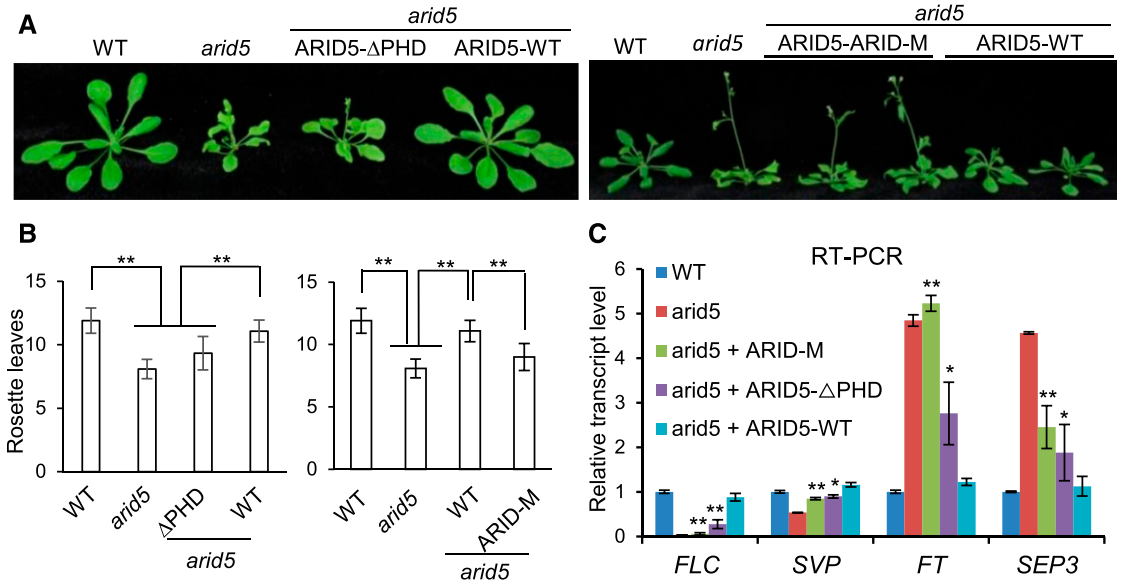

Figure 4. The ARID5 ARID-PHD Cassette Is Required for the Regulation of Development and Floral Transition.

(A) Morphological phenotypes of wild-type (WT) and *arid5* plants, and of transgenic plants expressing ARID5-WT, ARID5-ΔPHD, and ARID5-ARID-M in the *arid5* mutant background. Plants were photographed when the *arid5* mutant plants were bolting.

(B) The number of rosette leaves in the indicated genotypes. At least 20 plants for each genotype were included for the analysis. Asterisks indicate that the differences between the two indicated samples were statistically significant. Two-tailed student's *t* test: $^{**}P < 0.01$.

(C) Effect of the disruption of the PHD and ARID domains on the expression of *FLC*, *SVP*, *FT*, and *SEP3*. The expression of the indicated genes was assessed by RT-qPCR. The results are from three biological replicates. Error bars denote SD. The difference of gene expression between the ARID5-WT and ARID5-ΔPHD or ARID5-ARID-M transgenic plants was determined by two-tailed student's *t* test. $^{**}P < 0.01$; $^{*}P < 0.05$.

(Supplemental Figure 10). These results strongly suggest that both the PHD and the ARID domains are required for the function of ARID5 in Arabidopsis.

Structure of the ARID5-H3K4me3-DNA Ternary Complex

To further investigate the molecular mechanism of the interaction among ARID5, the H3K4me3 histone mark, and AT-rich DNA, we determined the crystal structure of both the ARID5 PHD finger in complex with an H3K4me3 peptide at 1.9-Å resolution and the ARID5 ARID-PHD fusion cassette in complex with a central AT-containing DNA and an H3K4me3 peptide at 1.5-Å resolution (Figure 5A; Supplemental Figure 11A; Supplemental Table 3). The superimposition of the two structures shows almost identical structures of the PHD finger segments with an root-mean–square deviation 0.62 Å, and the two peptides also adopt almost identical conformations (Supplemental Figures 11B and 11C). Because of the higher resolution and the greater number of components in the ARID-PHD-H3K4me3-DNA ternary complex structure, we will only refer to that complex in the following discussion.

Overall, the ARID and PHD domains are located side-by-side and form a compact dual-domain cassette. The DNA packs on one side of the dual-domain cassette, forming a major interaction with the ARID domain and a minor interaction with the PHD finger. The H3K4me3 peptide binds between the PHD and ARID domains without directly interacting with the DNA (Figure 5A). The H3K4me3 peptide fits into a narrow negatively charged surface cleft between the ARID and PHD domains, while the DNA interacts with a continuous positively charged surface of ARID5 (Figure 5B). Instead of being direct, the interactions between the ARID and PHD domains are mainly mediated by the histone peptide. The interface between the ARID and PHD domains only buries ~224.6 $Å^2$ of the surface area of each domain, which is relatively small and of hydrophilic nature. The majority of the interactions focus on a loop on the PHD finger to form several hydrogen bonds with the ARID domain (Figure 5C).

Combinatorial Readout of H3K4me3 by PHD and ARID Domains of ARID5

In the ARID-PHD-H3K4me3-DNA complex, the peptide possesses substantial electron density and can be built from H3A1 to H3T6 (Supplemental Figure 11D). The peptide interacts with the PHD and ARID domains with a binding surface area of 445.4 $Å^2$ and 309.9 $Å^2$, respectively. The PHD finger resembles other classic H3K4me3-recognition PHD fingers and interacts with the peptide from one side (Li and Li, 2012), while the ARID domain contributes less to peptide recognition and interacts with the peptide from the opposite side (Figures 5A and 5B). In detail, the amino group and the side-chain methyl group of H3A1 are anchored by two hydrogen bonds and by a shallow hydrophobic pocket of the PHD finger of ARID5, respectively (Figure 5D). The

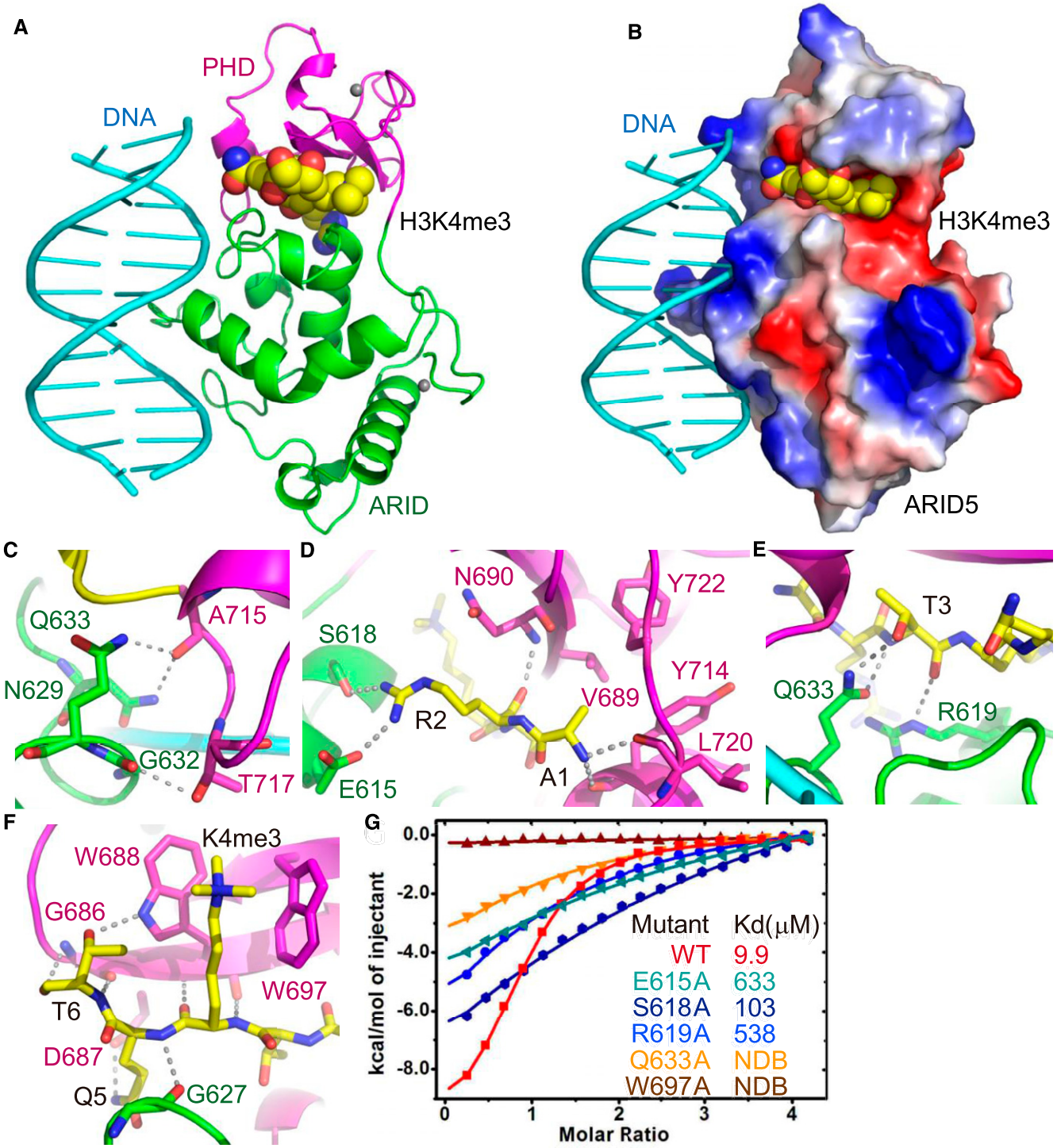

Figure 5. Structure of the ARID5 ARID-PHD Cassette in Complex with an H3K4me3 Peptide and DNA.

(A) Overall structure of the ARID5 ARID-PHD cassette in complex with an H3K4me3 peptide and an AT-containing DNA duplex. The ARID domain, PHD finger, and the DNA are colored green, magenta, and cyan, respectively. The peptide is shown in space-filling representation.

(B) An electrostatics surface view of the ARID5 ARID-PHD cassette with the H3K4me3 peptide and an AT-containing DNA in space-filling and cartoon representations, respectively.

(C) The interactions between the ARID and PHD domains with the interacting residues highlighted in stick representation. The hydrogen bonds are shown in dashed silver lines.

side chain of H3R2 forms hydrogen bonds with Ser618 and Glu615 of the ARID domain, and the side chain of H3T3 forms hydrogen bonds with Gln633 of the ARID domain (Figures 5D and 5E). The trimethyllysine of H3K4me3 is accommodated by an aromatic cage formed by PHD finger residues Trp688 and Trp697 (Figure 5F), which is similar to other classic methyl-lysine readers (Patel, 2016). The side chain of H3Q5 and H3T6 possess specific hydrogen-bonding interactions with Asp687 and Trp688, respectively (Figure 5F). Besides the side-chain recognition, the main chain of the H3K4me3 peptide forms a series of hydrogen-bonding interactions with both the ARID and PHD domains (Figures 5D to 5F).

In addition to the PHD finger, the ARID domain is also involved in the H3K4me3 peptide recognition, which raises the possibility that the two domains of ARID5 can combinatorially recognize the H3K4me3 mark. In our ITC-based binding assay, the binding affinity to the H3K4me3 peptide was 3-fold lower for the isolated PHD finger than for the ARID-PHD cassette (Supplemental Figure 11E), confirming the combinatorial readout. We then used this fused dual-domain cassette as a template to generate several mutants to disrupt the key residues involved in peptide binding. All of the key residue mutants, whether on the ARID domain or on the PHD finger, showed significantly decreased binding (Figure 5G), confirming the importance of the key residues on both domains.

Recognition of the AT-Containing DNA by the ARID Domain of ARID5

All the 12-bp DNA used in the crystallization can be observed in the final structure (Figure 5A). The DNA is mainly captured by the ARID domain with minor contributions from the PHD finger (Figures 5A and 5B). The majority of the interaction involves the backbone of the DNA (Figure 6A). Three loops of the ARID domain—Val601-Ser604, Asn626-Lys631, and Arg646-Lys655—contribute to the DNA recognition (Figure 6A). In particular, the Val601-Ser604 loop mainly forms hydrogen-bonding interactions with the phosphate groups of Thy3 and Ade4 of the forward DNA strand (Figure 6B). The phosphate groups of Ade4′, Gua5′, and Ade6′ of the complementary strand DNA are specifically recognized by an extensive hydrogen-bonding interaction network with the loop Asn626-Lys631 and Arg646-Lys655 of the ARID domain (Figure 6C). The phosphate group of Ade6 is specifically recognized by Arg646 with hydrogen-bonding and salt-bridge interactions (Figure 6D). The base-specific recognition occurs at Ade6 and Ade6′. The loop Arg646-Lys655 inserts into the major groove of the DNA (Figure 6E). At the tip of the loop, Thr648 forms two hydrogen bonds with the Hoogsteen edge of Ade6 by its side-chain hydroxyl group (Figures 6D and 6E). In addition, the main chain carbonyl group of Thr648 forms a hydrogen bond with the N6 of Ade6′ at the complementary strand.

When the Ade6 and Ade6′ are replaced by guanine, both the O6 and N7 of the guanine can only act as hydrogen acceptors and not as donors. As a consequence, only one hydrogen bond can be formed between the Ade6 and the side chain of Thr648, and no hydrogen bond can be formed between Ade6′ and the main-chain carbonyl of Thr648. We therefore concluded that the ARID domain of ARID5 specifically recognizes the central AT dinucleotide pairs to achieve the sequence preference, which is similar to other reported ARID domain-DNA complexes, such as Drosophila dead ringer (Iwahara et al., 2002; Cai et al., 2007).

Our further ITC measurements showed that the binding affinity was greatly reduced when the central AT motif was replaced with TA, CG, or GC (Figure 3D). In addition to the ARID domain, the Thr717 of the PHD finger also contributes to the DNA recognition with a hydrogen bond, indicating a minor role for the PHD finger in DNA binding (Figure 6C).

ARID5 Associates with H3K4me3-Enriched Genic Regions

Given that ARID5 can bind to H3K4me3 in vitro, we investigated whether ARID5 co-localizes with H3K4me3 on chromatin in vivo. We performed chromatin immunoprecipitation (ChIP) combined with deep sequencing (ChIP-seq) using *ARID5-GFP* transgenic plants in the *arid5* mutant background to determine the ARID5 occupancy at the whole-genome level. Based on two biological replicates of the ChIP-seq experiment, we identified 3,167 ARID5 peaks at the whole-genome level (Supplemental Data Set 3). Most of the ARID5 peaks (97.4%) overlapped with gene bodies, but not with promoters and intergenic regions (Figure 7A). The ARID5 peaks corresponded to 2,864 genes (Supplemental Data Set 3), which we termed ARID5-enriched genes.

We identified 14,781 H3K4me3-enriched genes based on previous H3K4me3 ChIP-seq data (Chica et al., 2013). Notably, the ARID5-enriched genes significantly (89.9%, 2575/2864, $P \rightarrow 0$, hypergeometric test) overlapped with the H3K4me3-enriched genes (Figure 7B). The ARID5 signals were primarily enriched in the gene body proximal to the transcription start site (TSS); the ARID5 pattern on the genic region was similar to the H3K4me3 pattern (Figures 7C and 7D). Moreover, the intensity of ARID5 signals was clearly correlated with that of H3K4me3 signals at the 5′ region of ARID5-enriched genes (Supplemental Figure 12). The H3K4me3 level was significantly higher in ARID5-enriched genes than in genes that are not enriched with ARID5 (Figure 7E). These analyses suggest that ARID5 specifically binds to genic regions that are highly enriched with H3K4me3, supporting the notion that H3K4me3 is necessary for the association of ARID5 with chromatin.

Given that the ARID domain of ARID5 can bind to AT-containing DNA as determined by in vitro binding assays and crystal structure analyses (Figures 3B, 3D, and 6A to 6E), it is of interest to

Figure 5. (continued).

(D) to **(F)** The specific recognition of H3A1, H3R2 **(D)**, H3T3 **(E)**, H3K4me3, H3Q5, and H3T6 **(F)** by AIRD5. The interacting residues are highlighted in stick representation. The hydrogen bonding interactions are highlighted by dashed silver lines.

(G) As determined by the ITC assay, mutations of the peptide interacting residues from both PHD and ARID domains significantly decrease the binding affinity between the ARID5 and the H3K4me3 histone mark.

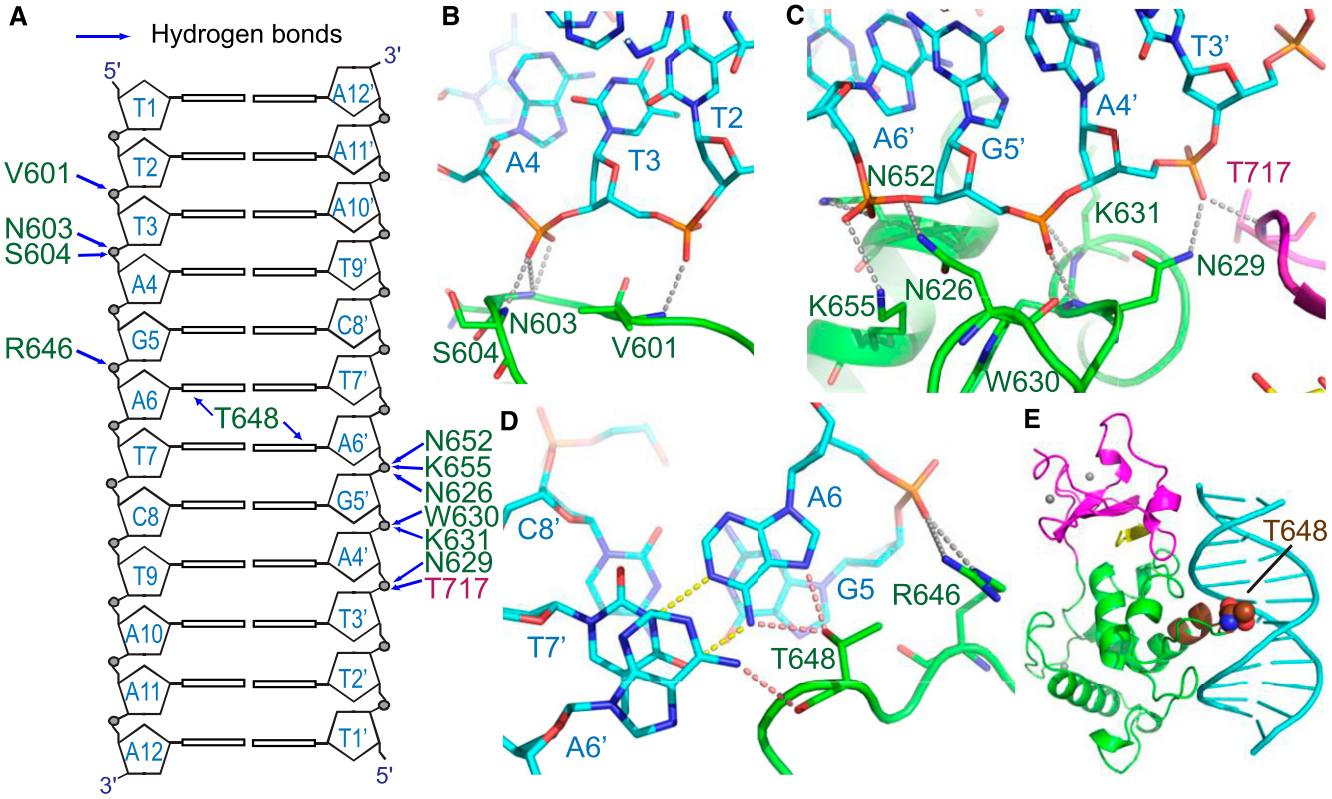

Figure 6. Specific Recognition of the AT-Containing DNA by ARID5.

(A) A schematic representation of the interactions between ARID5 and AT-containing DNA. The hydrogen bonding interactions are highlighted by blue arrows. The interacting residues are marked in green and magenta for ARID domain and PHD domain residues, respectively.
(B) to **(D)** The specific hydrogen bonding interactions between ARID5 and the forward-strand DNA residues T3 and A4 **(B)**, the reverse-strand DNA residues A4′, G5′, and A6′ **(C)**, and the base-specific interaction between Thr648 and the central AT dinucleotides of the DNA and the interaction between Arg646 and the backbone phosphate group of A6 **(D)**. The base-specific interacting hydrogen bonds, base-pairing hydrogen bonds, and phosphate-interacting hydrogen bonds are highlighted in red, yellow, and silver dashed lines, respectively. All of the interacting residues are highlighted in stick representation.
(E) The Thr648 of loop Arg646-Lys655 inserts into the major groove of the DNA duplex and thereby directly interacts with the DNA base. The loop is highlighted in brown with Thr648 in space-filling representation.

determine whether the association of ARID5 with chromatin depends on the recognition of a sequence-specific motif in vivo. By carrying out a motif discovery analysis using the ARID5 ChIP-seq data (Heinz et al., 2010), we identified RAATCGAW (R represents A and G; W represents A and T) as the most significantly enriched ARID5-bound motif (Figure 7F; Supplemental Table 4). Interestingly, this motif is best matched to the known ARID3-bound motif as determined by a previous in vitro DNA motif analysis (O'Malley et al., 2016), suggesting that the DNA binding ability of the ARID domains in ARID3 and ARID5 is conserved. We found that the ARID5-bound motif-centered genomic regions form an H3K4me3 peak but not a peak of H3K9me2, which is highly enriched at heterochromatin regions (Figure 7F). This analysis suggests that the association of ARID5 with chromatin may depend on both H3K4me3 and the AT-containing DNA motif.

ARID5 Associates with Chromatin through the PHD and ARID Domains and Is Involved in the Association of the CRA-Type ISWI Complex with Chromatin and in Transcriptional Regulation

We investigated whether the PHD and ARID domains are required for the association of ARID5 with chromatin in vivo. Using ChIP combined with quantitative PCR (ChIP-qPCR), we compared the association of the GFP-tagged ARID5-WT, ARID5-ΔPHD, and ARID5-ARID-M with five representative ARID5-enriched genes as identified by ChIP-seq (Supplemental Figure 13). ChIP-qPCR confirmed the enrichment of ARID5 at these genes, suggesting that our ChIP-seq results are reliable (Figure 8A). The occupancy of ARID5-ΔPHD and ARID5-ARID-M at these genes was markedly decreased (Figure 8A), indicating that both PHD and ARID domains are required for the association of ARID5 with chromatin in vivo.

Given that the ARID5-enriched genes are identified, it is of interest to investigate whether the other subunits of the CRA-type ISWI complex associate with the ARID5-enriched genes. We performed ChIP-qPCR for CHR11 and RLT2 using *CHR11-Flag* and *RLT2-Flag* transgenic plants, respectively. The result indicated

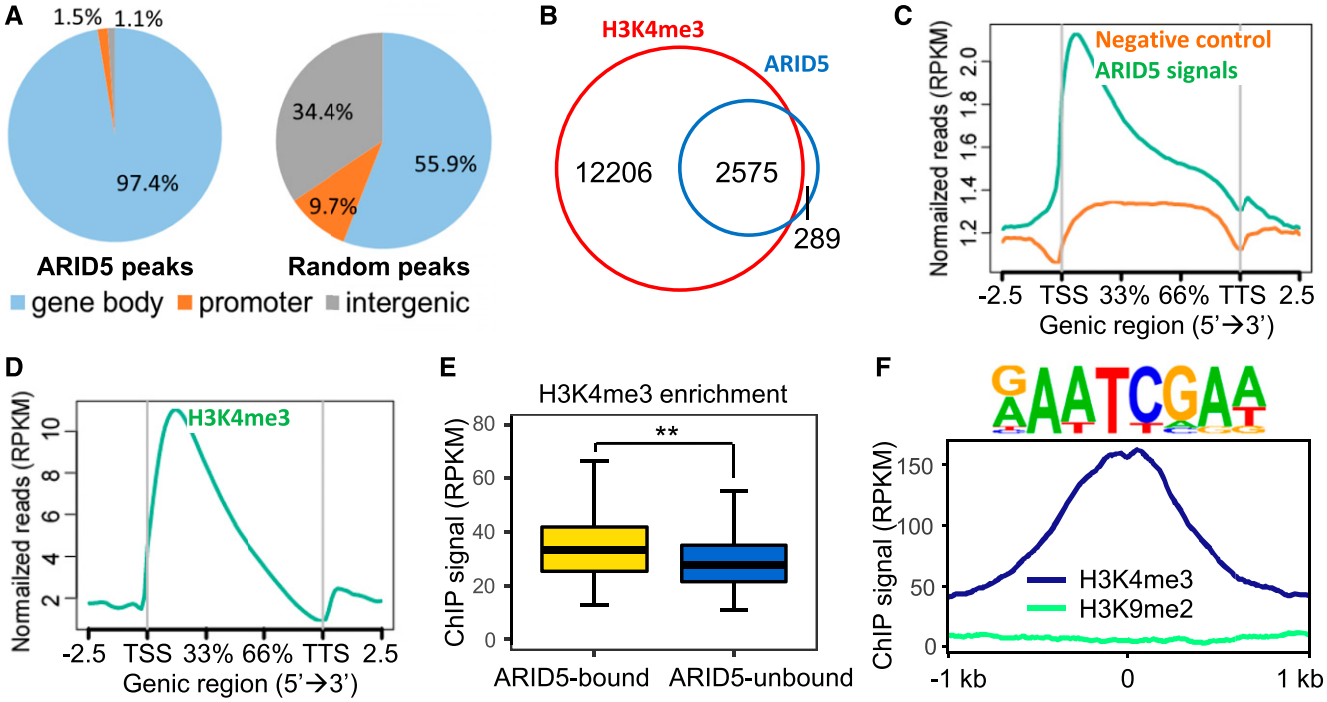

Figure 7. Characterization of ARID5-Bound Chromatin Regions as Determined by ARID5 ChIP-Seq.

(A) Distribution of ARID5 peaks and random peaks on the genome. Random peaks refer to the same number of random genomic regions as ARID5 peaks.
(B) Venn diagram showing the overlap between ARID5- and H3K4me3-enriched genes.
(C) and **(D)** Metaplots showing average ARID5 **(C)** and H3K4me3 **(D)** levels on the transcription units of ARID5-bound genes. The TSS and the transcription termination site (TTS) are shown on the X axis. −2.5, 2.5-kb region upstream of TSS; 2.5, 2.5-kb region downstream of TTS. RPKM, Reads Per Kilobase of transcript, per Million mapped reads.
(E) Box plots showing H3K4me3 levels in ARID5-bound H3K4me3-enriched genes and ARID5-unbound H3K4me3-enriched genes. Center lines (median), interquartile ranges, and whiskers (± 1.5 × interquartile ranges) are shown in the box plots.
(F) The most significantly ARID5-enriched motif is shown at the top; H3K4me3 and H3K9me2 profiles in the motif-centered genomic regions are shown at the bottom.

that CHR11 and RLT2 can associate with the ARID5-enriched genes tested in this study (Figure 8B), suggesting that ARID5 may associate with chromatin in the form of the CRA-type ISWI complex. To determine whether the association of ARID5 with chromatin is necessary for the occupancy of the ISWI complex, we introduced the *arid5* mutation into the *CHR11-Flag* transgenic plants and then tested the effect of *arid5* on the association of CHR11 with chromatin. We found that the *arid5* mutation partially reduced the association of CHR11 with the ARID5-bound genes (Figure 8C), suggesting that ARID5 is at least partially responsible for the association of the CRA-type ISWI complex with certain specific chromatin loci.

To determine whether the association of ARID5 with chromatin is involved in the regulation of gene expression, we analyzed the expression levels of the ARID5-bound genes using the RNA-seq data and found that the expression of a part of ARID5-bound genes were either up- or downregulated in the *arid5*, *rlt1/2*, and *chr11/17* mutants (Supplemental Figure 14A), suggesting that ARID5 may either activate or repress gene expression. To investigate how ARID5 regulates gene expression, we introduced the *arid5* mutation into transgenic plants harboring a *CaMV 35S* promoter-driven luciferase reporter gene (*35S-LUC*), which were termed *YJ* in a previous study (Li et al., 2016b), and analyzed the effect of *arid5* on the *35S-LUC* expression. The result indicated that the *arid5* mutation markedly reduced the *35S-LUC* expression (Figures 8D and 8E), suggesting that ARID5 can mediate transcriptional activation.

Furthermore, by analyzing the H3K4me3 ChIP-seq data, we found that the enrichment of H3K4me3 was significantly higher in the downregulated genes than in the upregulated genes (Supplemental Figure 14B), supporting the notion that ARID5 associates with H3K4me3-enriched genes and functions as a transcriptional activator. However, given that the expression of ARID5-bound genes can be either up- or downregulated in the *arid5* mutant (Supplemental Figure 14A), we cannot exclude the possibility that ARID5 may also function as a transcriptional repressor in vivo. The involvement of ARID5 in activation or repression may depend on the genomic context or co-regulators.

DISCUSSION

Although the ISWI complexes in yeast and animals have been identified and characterized, relatively little is known about the ISWI complexes in plants (Li et al., 2017). Here, we identified three

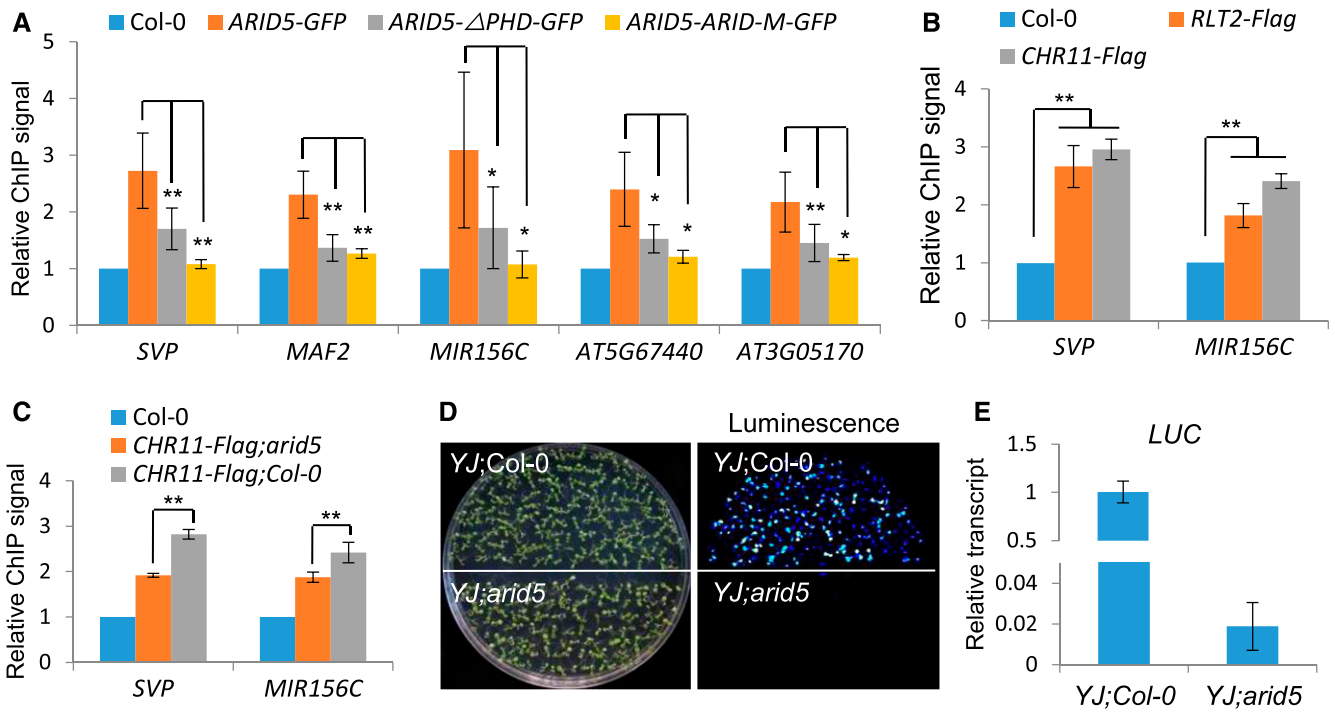

Figure 8. ARID5 Associates with Chromatin through the PHD and ARID Domains and Is Involved in the Association of CHR11 with Chromatin and in Transcriptional Activation.

(A) The enrichment of ARID5-WT, ARID5-ΔPHD, and ARID5-ARID-M in ARID5 target loci as determined by ChIP-qPCR. Values are mean ± SD. The difference of the enrichment between the ARID5-WT and ARID5-ΔPHD or ARID5-ARID-M transgenic plants was determined by Student's *t* test. **P < 0.01; *P < 0.05.
(B) Determination of the association of CHR11-Flag and RLT2-Flag with *SVP* and *MIR156C* by ChIP-qPCR in the *CHR11-Flag* and *RLT2-Flag* transgenic plants and the wild-type plants. Values are mean ± SD. **P < 0.01 as determined by Student's *t* test.
(C) The association of CHR11-Flag with *SVP* and *MIR156C* in the *arid5* mutant and wild-type Col-0 backgrounds as determined by ChIP-qPCR. Values are mean ± SD. **P < 0.01 as determined by Student's *t* test.
(D) The photograph and luminescence imaging of seedlings carrying the *CaMV 35S* promoter-driven luciferase transgene (*YJ*) in the wild-type Col-0 and *arid5* mutant backgrounds.
(E) Determination of the expression levels of *35S-LUC* by RT-qPCR. Values are means ± SD from three biological replicates.

types of ISWI complexes—CRA, CDM, and CDD. The CDD-type ISWI complex contains two subunits, i.e., the ISWI protein and the DDT-domain protein, whereas the CRA- and CDM-types of ISWI complexes contain at least three subunits composed of not only the ISWI protein and the DDT-domain protein but also ARID5 and MSI3, respectively. This study has therefore identified different types of ISWI complexes in Arabidopsis. Unlike other types of ISWI complexes, the CRA-type ISWI complex contains ARID5, an ARID-domain protein. ARID5 represents a unique member of the ARID-domain protein family and is characterized by a PHD finger (Zhu et al., 2008). The ARID domain is present in several chromatin-related proteins in eukaryotes (Fleischer et al., 2003; Klose et al., 2006; Mashtalir et al., 2018), but here we show that ARID5 functions as a subunit of ISWI complexes. Given that ARID5 is highly conserved in plants, our study suggests that CRA may represent a plant-specific type of ISWI complex.

Our results indicated that the chromatin-remodeling regulators CHR11/17 are shared catalytic subunits of three different types of ISWI complexes (Figure 1A; Supplemental Table 1). Therefore, it is reasonable to predict that the phenotypic defect in the *chr11/17* mutant is stronger than that in the mutants depleted in subunits of a specific ISWI complex. Consistent with the prediction, the phenotypic defect in the *chr11/17* mutant is clearly stronger than that in the *rlt1/2* and *arid5* mutants, supporting the scenario that CHR11/17 cannot only function as subunits of the CRA-type ISWI complex but also as subunits of two other types of ISWI complexes. In the future, it will be interesting to investigate the biological function of the other types of ISWI complexes and to determine how the different types of ISWI complexes function cooperatively to regulate chromatin states and gene expression during diverse biological processes.

The PHD finger is present in several DDT-domain subunits of ISWI complexes and facilitates the association of the ISWI complexes with H3K4me3-enriched chromatin in Drosophila and mammals (Xiao et al., 2001; Li et al., 2006; Wysocka et al., 2006). In the Arabidopsis DDT-domain protein family, only DDP1, DDP2, and DDP3 contain the PHD finger (Dong et al., 2013). DDP1, DDP2, and DDP3 were identified as subunits of the CDM-type of ISWI complex in our study. A previously reported in vitro assay demonstrated that DDP1/PTM can bind to H3K4me3 (Sun et al., 2011).

These previous results suggest that the association of the ISWI complexes with H3K4me3-enriched chromatin may be conserved among plants and animals. It is unknown, however, whether and how the ISWI complexes associate with H3K4me3-enriched chromatin when the PHD finger is absent in the DDT-domain subunits. In the CRA-type of ISWI complex, the PHD finger is present in the ARID-domain subunit ARID5 but not in the DDT-domain subunits RLT1 and RLT2. Our study suggests that the PHD finger of ARID5 is responsible for the association of ARID5 with H3K4me3-enriched chromatin loci. Therefore, the PHD finger of ARID5 in the CRA-type ISWI complex is functionally equivalent to that of the DDT-domain proteins in the other ISWI complexes. The study reveals a mechanism that mediates the association of ISWI complexes with H3K4me3.

In plants, the histone-mark readers share features with their animal counterparts but also have plant-specific features (Liu et al., 2018a). Here, we found that ARID5 can recognize the H3K4me3 mark by the contributions from both PHD and ARID domains. The PHD finger plays a dominant role in the recognition, and the ARID domain can significantly enhance the binding, indicating a combinatorial recognition of the H3K4me3 mark. In this combinatorial recognition system, the PHD finger is in charge of the recognition of H3A1, H3K4me3, and H3T6, while the ARID domain mainly interacts with H3R2, H3T3, and H3Q5. The PHD finger itself is sufficient for the recognition of the H3K4me3 mark, although the binding affinity is lower for the PHD finger alone than in combination with ARID. In the ARID-PHD dual-domain context, the interaction between the PHD finger and H3K4me3 is almost identical as the recognition of H3K4me3 by the isolated PHD finger. ARID only acts as an enhancer of the binding. This type of combinatorial readout of histone mark resembles the recognition of unmodified H3 peptide by the Arabidopsis ORC1b BAH-PHD cassette (Li et al., 2016c), in which the PHD finger provides the major contribution to the unmodified H3 peptide recognition and the BAH domain enhances the binding by binding to the other side of the peptide.

Our study demonstrates that the ARID5 ARID-PHD cassette can function as a dual-recognition module for H3K4me3 and AT-containing DNA. The binding affinity of the ARID-PHD cassette to the H3K4me3 peptide is comparable to the DNA, indicating that the protein–DNA and protein–histone interactions are equally important. Our ARID5 ChIP-seq data demonstrate that both H3K4me3 and AT-containing DNA are characteristics of ARID5-bound regions, supporting the notion that the dual recognition of H3K4me3 and AT-containing DNA may cooperatively determine the targeting specificity of ARID5. Besides Arabidopsis ARID5, there are many human proteins containing the fused ARID-PHD cassette, such as RBP2, PLU-1, and SMCX (Wilsker et al., 2002). There have been no structural studies of the reading of histone marks by these proteins in humans. It follows that our structural studies of the ARID5 ARID-PHD cassette in the dual recognition of H3K4me3 peptide and DNA in Arabidopsis may provide insight into those proteins in humans.

Considering that ARID5 is only partially responsible for the association of the CRA-type ISWI complex with chromatin (Figure 8C), we predict that CHR11/17 (shared catalytic subunits of different types of ISWI complexes) may directly bind to chromatin and then provide a basic binding affinity to chromatin. The recognition of ARID5 to H3K4me3 and AT-containing DNA is likely to add a targeting specificity for the CRA-type ISWI complex. Similarly, we suspect that the association of the other types of ISWI complexes with specific chromatin loci may also depend on their unique subunits. Moreover, considering that the floral transition is a dynamic process, we speculate that the association of the CRA-type ISWI complex with chromatin may be regulated by internal or environmental signals. In the future, it will be interesting to investigate whether and how the association of the ISWI complex with chromatin is dynamically modulated.

METHODS

Plant Materials and Growth

The Arabidopsis (*Arabidopsis thaliana*) T-DNA insertion mutants *arid5* (SALK_111627), *rlt1* (SALK_099250), *rlt2* (SALK_132828), *chr11* (GK-424F01), and *chr17* (SALK_080144) were obtained from the Arabidopsis Biological Resource Center. The double mutants *rlt1/2* and *chr11/17* were generated by crossing. Arabidopsis seeds were sown on Murashige-and-Skoog–medium plates and kept in 4°C for 2 d, and then grown under the condition of 16 h of light (100 μmol/m^2/s provided by white-light fluorescent tubes [F17T8/TL841; Philips]) at 23°C and 8 h of darkness at 21°C. After grown for 10 d, the Arabidopsis seedlings were used for RNA-seq and ChIP-seq or transferred to soil for further experiments. The genotyping primers are listed in Supplemental Data Set 4.

Constructs and Transformation

For generation of the *ARID5-WT* construct, the full-length *ARID5* genomic sequence without the stop codon (1 to 4,406 bp) driven by a 1.5-kb native promoter was introduced into the modified *pCAMBIA1305* vector to express the C-terminal *5×Myc*- or *GFP*-tagged *ARID5* transgenes. For generation of the *ARID5-ΔPHD* construct, the truncated *ARID5* genomic sequence (1 to 4,021 bp) without the 3′-terminal sequence encoding the PHD domain was cloned. For generation of the *ARID5-ARID-M* construct, site-directed mutagenesis was performed to introduce point mutations (P598A and W630A) into the ARID domain of ARID5. Both the *ARID5-ΔPHD* and *ARID5-ARID-M* sequences were driven by the same promoter and cloned into the same vector as the *ARID5-WT* sequence. The full-length genomic sequences of *RLT1*, *RLT2*, *CHR11*, *CHR17*, *MSI3*, *DDR1*, *DDR3*, *DDR4*, *DDR5*, *DDP2*, *DDP3*, and *DDW1* without the stop codon driven by corresponding 1.5-kb native promoters were introduced into the modified *pCAMBIA1305* or *pRI909* vectors to express the C-terminal *5×Myc* or *3×Flag*-tagged proteins. Primers used for the construction are listed in Supplemental Data Set 4. The constructs were transformed into the wild-type Col-0 plants or into corresponding mutant plants by Agrobacterium-mediated infection. The T1 transgenic plants were grown on Murashige-and-Skoog plates with 30 mg/L of hygromycin and the resistant-positive seedlings were selected for further analysis.

Affinity Purification, Mass Spectrometric Analysis, Co-IP, and Gel Filtration

For affinity purification, a 3-g quantity of seedlings or flowers was ground in liquid nitrogen and homogenized in 15 mL of lysis buffer (50 mM of Tris-HCl at pH 7.6, 150 mM of NaCl, 5 mM of $MgCl_2$, 10% [v/v] glycerol, 0.1% [v/v] NP-40, 0.5 mM of DTT, 1 mM of PMSF, and Roche protease inhibitor cocktail). After the homogenate was centrifuged at 12,000*g* and 4°C for 15 min, the supernatant was filtered through two layers of Miracloth (EMD Millipore) and incubated with 100 μL of Anti-Flag M2 Affinity Gel (cat. no. A2220; Sigma-Aldrich) or Anti-c-Myc Agarose Affinity Gel (cat. no. A7470;

Sigma-Aldrich) at 4°C for 2.5 h. The preparation was then washed five times with the lysis buffer, and the Flag-beads–bound proteins were eluted with 3 μL of 3×Flag peptide (cat. no. F4799; Sigma-Aldrich), whereas the Myc-beads–bound proteins were eluted with 100 μL of 0.1-M ammonium hydroxide. The eluted proteins were run on an SDS-PAGE gel and then subjected to silver staining with a ProteoSilver Silver Stain Kit (PROTSILI-1KT; Sigma-Aldrich).

The mass-spectrometric (MS) analysis was performed as previously described by Zhang et al. (2013). Protein bands on the SDS-PAGE gel were destained, and then reduced in 10 mM of DTT at 56°C for 30 min followed by alkylation in 55 mM of iodoacetamide at dark for 1 h. After that the protein bands were in-gel–digested with sequencing-grade trypsin (10 ng/μL of trypsin and 50 mM of ammonium bicarbonate at pH 8.0) overnight at 37°C. Peptides were extracted with 5% (v/v) formic acid/50% (v/v) acetonitrile and 0.1% formic acid/75% acetonitrile sequentially and then concentrated to ~20 μL. The extracted peptides were separated by an analytical capillary column (50 μm × 15 cm) packed with 5 ìm of spherical C18 reversed-phase material (YMC). A nanoAcquity UPLC system (Waters) was used to generate the following high-performance liquid chromatography gradient: 0 to 30% (v/v) B in 40 min, 30 to 70% (v/v) B in 15 min (A = 0.1% [v/v] formic acid in water, B = 0.1% [v/v] formic acid in acetonitrile). The eluted peptides were sprayed into a QE Mass Spectrometer (Thermo Fisher Scientific) equipped with a nano-electrospray ionization ion source. The mass spectrometer was operated in data-dependent mode with one MS scan followed by four Collision-Induced Dissociation and four High-Energy Collisional Dissociation MS/MS scans for each cycle. Database searches were performed on an in-house Mascot server (Matrix Science) against the international protein index database.

For performing co-IP, *Flag*- and *Myc*-tagged transgenic plants were crossed to obtain F1 generation seedlings expressing two different tagged proteins. Proteins were extracted from the F1 seedlings and parent seedlings for affinity purification. The input and eluted proteins were run on an SDS-PAGE gel for immunoblotting and were detected using anti-Flag (cat. no. F1804; Sigma-Aldrich) and anti-Myc (cat. no. M20002; Abmart) antibodies diluted at 1:5,000.

For gel filtration, 0.4 g of seedlings was ground and suspended in 2.4 mL of lysis buffer. After centrifugation, the supernatant was passed through a 0.22-μm filter, and 500 μL of the filtrate was loaded onto a Superose 6 increase column (10/300 GL; model no. 29-0915-96; GE Healthcare Life Sciences). The eluate was collected in a series of fractions and run on an SDS-PAGE gel for immunoblotting.

Y2H Analysis

The full-length coding sequences of *ARID5*, *CHR11*, *CHR17*, *RLT1*, *RLT2*, *DDP1*, *DDP2*, *DDP3*, *DDW1*, *DDR1*, *DDR3*, *DDR4*, *DDR5*, and *MSI3* and the truncated coding sequences of *ARID5* and *RLT2* were cloned into *pGADT7* (with *GAL4-AD*) and/or *pGBKT7* (with *GAL4-BD*) vectors using a One-Step Cloning Kit (C112; Vazyme Biotech). Primers used for the cloning are listed in Supplemental Data Set 4. The yeast strains AH109 and Y187 were transformed with the *GAL4-AD* and *GAL4-BD* constructs, respectively. After mating, Y2H assays were performed on synthetic dropout (SD) medium lacking Trp, Leu, and His, supplemented with 3-amino-1,2,4-triazol. The program Cytoscape 3.1.0 (http://cytoscape.org) was used for visualizing interaction networks.

RNA Transcript Analysis

One gram of 10-d–old Col-0, *arid5*, *rlt1/2*, and *chr11/17* Arabidopsis seedlings were collected for each biological replicate. Trizol reagent (Invitrogen) was used for extraction of total RNA. Total RNA was sent to BGI for library preparation and sequencing. The presented data were obtained from two independent biological experiments. For RNA-seq data analysis, we removed the adapter sequences and trimmed the low-quality bases using the software SOAPnuke v1.5.2 (Cock et al., 2010). The clean reads were then aligned to The Arabidopsis Information Resource (TAIR10) genome using the software HISAT2 v2.0.4 (Kim et al., 2015). DEGs were identified using the tool DEGseq (fold-change ≥ 2, and adjusted P-value $\leq$ 0.001; Wang et al., 2010). The heatmap of DEGs was drawn using the heatmap.2 function in the gplots R package. The expression changes of flowering-time genes in the *arid5*, *rlt1/2*, and *chr11/17* mutants relative to the wild type were subjected to correlation analysis using the geom_point function in the software package ggplot2 R (https://cran.r-project.org). The RNA-seq signals were visualized by JBrowse (https://github.com/GMOD) as reported in Buels et al. (2016). For RT-qPCR, total RNA was treated with DNase I (M0303S; New England BioLabs) to remove DNA. The reverse-transcription product (cDNA) was generated using a reverse transcription kit (RR037A; Takara). The cDNA was used for RT-qPCR. qPCR was performed using SYBR FAST qPCR Master Mix (KR0389; KAPA). The results shown in the study were generated from three biological replicates.

ChIP

ARID5-GFP transgenic plants in the *arid5* mutant background were used for ChIP-seq. Myc-tagged *ARID5-WT*, *ARID5-ΔPHD*, and *ARID5-ARID-M* transgenic plants were used for ChIP-qPCR. The wild-type Col-0 plants were used as a negative control in both ChIP-seq and ChIP-qPCR. ChIP assays were performed as previously described with minor modification (Liu et al., 2018b). In brief, a 2-g quantity of 10-d–old Arabidopsis seedlings was ground into powder and cross linked with 1% (v/v) formaldehyde (cat. no. F8775; Sigma-Aldrich) in 15 mL of lysis buffer (20 mM of Tris-HCl at pH 7.5, 20 mM of KCl, 2 mM of EDTA at pH 8.0, 2.5 mM of $MgCl_2$, 25% [v/v] glycerol, 250 mM of Suc, 5 mM of DTT, 0.1 mM of PMSF, and Roche protease inhibitor cocktail) for 20 min at 4°C. The homogenate was filtered through two layers of Miracloth (EMD Millipore) and pelleted by centrifuging at 1,500*g* and 4°C for 10 min. The pellet was washed with nuclei resuspension buffer (20 mM of Tris-HCl at pH 7.5, 2.5 mM of $MgCl_2$, 25% [v/v] glycerol, and 0.2% [v/v] Triton X-100) until the pellet was no longer green. Then the nuclei were resuspended in nuclear lysis buffer (20 mM of Tris-HCl at pH 8.0, 2 mM of EDTA, 0.2% [v/v] NP-40, 1 mM of PMSF, and Roche protease inhibitor cocktail tablets). Chromatin was sonicated to a range of sizes from 200 bp to 500 bp using a Bioruptor (Diagenode). After centrifugation at 16,000*g* for 15 min, the supernatant was diluted 2-fold with dilution buffer (20 mM of Tris-HCl at pH 8.0, 2 mM of EDTA, 200 mM of NaCl, 1 mM of PMSF, and Roche protease inhibitor cocktail tablets). Laboratory-prepared GFP beads or Myc antibody (cat. no. ab32; Abcam) were used to immunoprecipitate the protein–DNA complex. The protein–DNA complex was reverse cross linked at 65°C and treated with proteinase K and RNase. The DNA was then purified for qPCR or sequencing.

For ChIP-seq, DNA was sent to Novogene for library preparation and sequencing. Two biological replicates were performed. For analysis of ChIP-seq data, the clean reads were mapped to the TAIR10 Arabidopsis genome with the software BowTie2 v2.2.5 (Langmead and Salzberg, 2012). The program macs2 callpeak was used to identify peaks (Zhang et al., 2008). The program macs2 bdgdiff was used to determine peaks that were differentially expressed between wild-type and mutant plants. The software ngs.plot v2.61 was used to draw Meta plots showing the average levels of ARID5 and H3K4me3 around the transcription units of ARID5-bound gene (Shen et al., 2014). The ARID5-enriched motif was identified by the HOMER v4.9.1 subroutine findMotifsGenome.pl with default parameters (Heinz et al., 2010). The profiles of H3K4me3 and H3K9me2 in the motif-centered genomic regions were plotted using the plotProfile function in the program deepTools 3.1.2 (Ramírez et al., 2014). The heatmap of ARID5 and H3K4me3 ChIP-seq signals around the TSS was plotted using the plotHeatmap function in deepTools 3.1.2 (Ramírez et al., 2014). The ARID5 and H3K4me3 ChIP-seq signals were visualized by JBrowse

(https://github.com/GMOD) as reported in Buels et al. (2016). qPCR was performed using SYBR FAST qPCR Master Mix (KR0389; KAPA). Primers used for ChIP-qPCR are listed in Supplemental Data Set 4.

Protein Expression, Purification, and Pull Down

The ARID-PHD cassette of Arabidopsis ARID5 (residues 545 to 747) was cloned in a modified *pET-Sumo* vector to fuse a hexahistidine tag and a yeast Sumo tag to the N terminus of the target protein. The plasmid was transformed into *Escherichia coli* strain BL21(DE3), and the cells were cultured in Luria Bertani medium. Protein expression was induced by adding isopropyl β-D-thiogalactoside (IPTG) to a final concentration of 0.2 mM when the OD_{600} of the cell culture reached 0.8. The recombinant expressed protein was purified sequentially by Ni-NTA, Heparin, and Superdex G200 columns (GE Healthcare Life Sciences). The PHD finger of ARID5 (residues 673 to 747) was cloned, expressed, and purified using the same protocol used for ARID-PHD. All of the mutations were generated by a PCR-based method and were expressed and purified using the same protocol used for wild-type protein. The peptides and oligos were purchased from GL Biochem and Sangon Biotech, respectively.

The *RLT2-N*, *RLT2-M*, and *RLT2-C* cDNAs were cloned into the *pGEX6P-1* vector with a glutathione S-transferase (GST) tag on their N termini, then expressed and purified in the DE3 *E. coli* strain. The *ARID5* cDNA was cloned into the *pET28a* vector with a 6-His tag on its N terminus. The *CHR11* cDNA with a Flag tag on its N terminus was cloned into the *pAT424* vector and then expressed in the *Saccharomyces cerevisiae* strain YPH499. For the pull-down assay, GST beads were incubated with 3 μg of the GST fusion protein, then washed and incubated with 3 μg of His- or Flag-tagged proteins overnight at 4°C. Mock controls included the GST protein expressed from the *pGEX6P-1* vector. After the incubation, the beads were washed five times with a solution containing 20 mM of Tris at pH 7.4, 150 mM of NaCl, and 0.05% (v/v) TWEEN 20, then separated on an SDS-PAGE gel and analyzed by immunoblotting using an anti-GST antibody (cat. no. M20007L; Abmart), anti-His antibody (cat. no. TA100013; ORIGENE), or anti-Flag antibody (cat. no. M20008L; Abmart) diluted at 1:5,000.

EMSA

EMSA was performed as previously described by Ning et al. (2015). In brief, 1 μg of purified protein was incubated with DNA probes in a binding buffer (25 mM of HEPES at pH 7.6, 50 mM of KCl, 0.1 mM of EDTA at pH 8.0, 12.5 mM of $MgCl_2$, 1 mM of DTT, 0.5% [w/v] BSA, and 5% [v/v] glycerol) at room temperature for 30 min. The binding reaction mixture was loaded onto a 7% non-denaturing polyacrylamide gel and run at 80 V for 2 h, and the bound DNAs were visualized by ethidium bromide staining.

In Vitro Histone Binding Assays

For pull-down assay, we added 1 μg of different biotinylated histone peptides to 300 μL of binding buffer with 1 μg of the GST-ARID5-PHD fusion protein. The mixture was rotated at 4°C for 4 h. We also incubated the fusion protein without the histone peptides as a negative control. Then, the mixture was incubated with 30 μL of Streptavidin MagneSphere Paramagnetic Particles (cat. no. Z5481; Promega) for 2 h with rotation. The beads were washed three times and resuspended in 30 μL of 2 × SDS sample buffer. The protein bound by the beads was boiled and subjected to SDS-PAGE. GST antibody (cat. no. M20007L; Abmart) diluted at 1:5,000 was used for detecting the GST-fusion protein. Histone peptides used in this study were H3 (1 to 21 amino acids; cat. no. 12-403; EMD Millipore), H3K4me1 (cat. no. 12-563; Millipore), H3K4me2 (cat. no. 12-460; EMD Millipore), H3K4me3 (cat. no. 12-564; EMD Millipore), H3K9me1 (cat. no. 81,045; Active Motif), H3K9me2 (cat. no. 810406; Active Motif), H3K9me3 (cat. no. 810407; Active Motif), H3 (21 to 44 amino acids; cat. no. 12-404; EMD Millipore), H3K27me1 (cat. no. 81,050; Active Motif), H3K27me2 (cat. no. 81,051; Active Motif), H3K27me3 (cat. no. 81,052; Active Motif), H3K36me1 (cat. no. 12-0022; EpiCypher), H3K36me2 (cat. no. 12-0023; EpiCypher), and H3K36me3 (cat. no. 12-0024; EpiCypher) .

The ITC-based binding assay was performed using a MicroCal PEAQ-ITC instrument (Malvern) at 25°C. The purified proteins were dialyzed overnight at 4°C and diluted to 0.1 mM with the dialysis buffer. The peptides or DNA oligos were dissolved in the same buffer and adjusted to 1.0 to 1.5 mM. Binding was performed using the standard protocol, and the data were fit using the program Origin 7.0 (https://www.originlab.com).

Crystallization and Structure Determination

For complex formation, the protein, the peptide, and the DNA oligo were mixed in a molar ratio of 1:4:1.5 at 4°C for 2 h before crystallization screening. The ARID5 ARID-PHD cassette in complex with H3K4me3 peptide and DNA was crystallized in a condition of 0.1 M of sodium acetate at pH 5.0 and 15% (v/v) (+/-)-2-methyl-2,4-pentanediol (MPD). The ARID5 PHD finger in complex with an H3K4me3 peptide was crystallized in condition of 0.1 M of sodium acetate at pH 4.6 and 30% (w/v) PEG300. The diffraction data were collected at the Shanghai Synchrotron Radiation Facility beamline BL19U and were further processed using the program HKL3000 (Otwinowski and Minor, 1997).

Both the structure of the ARID5 PHD finger in complex with H3K4me3 peptide and the structure of the ARID5 ARID-PHD cassette in complex with H3K4me3 peptide and DNA duplex were determined using the single-wavelength anomalous dispersion method as implemented in the program Phenix (Adams et al., 2010). The structures were refined using the programs Phenix and Refmac (Murshudov et al., 1997; Adams et al., 2010). Model building was performed using the software Coot (Emsley et al., 2010). All of the molecular graphics were prepared using the program PyMol (DeLano Scientific LLC). A summary of the statistics of the data collection and structure refinement is listed in Supplemental Table 3.

Accession Numbers

X-ray structures have been deposited in the Research Collaboratory for Structural Bioinformatics Protein Data Bank with the accession code 6LQE for the ARID5 PHD finger in complex with H3K4me3 peptide and 6LQF for the ARID5 ARID-PHD cassette in complex with H3K4me3 peptide and DNA. Raw RNA-seq and ARID5 ChIP-seq data have been deposited in the Gene Expression Omnibus database with the accession code GSE139638. Accession numbers of genes used in this study include: AT3G06400 (*CHR11*), AT5G18620 (*CHR17*), AT1G28420 (*RLT1*), AT5G44180 (*RLT2*), AT3G43240 (*ARID5*), AT4G35050 (*MSI3*), AT5G35210 (*DDP1*), AT5G22760 (*DDP2*), AT5G12400 (*DDP3*), AT5G38690 (*DDR1*), AT1G67780 (*DDR3*), AT1G18950 (*DDR4*), AT5G25580 (*DDR5*), and AT5G08630 (*DDW1*).

Supplemental Data

Supplemental Figure 1. The developmental defect in the *chr11/17* double mutant was complemented by the *CHR11-Flag* transgene.

Supplemental Figure 2. Analyses of ARID5 and its orthologs in plants.

Supplemental Figure 3. The interaction of subunits of ISWI complexes as determined by Y2H assays.

Supplemental Figure 4. The interaction of RLT2 with a series of truncated ARID5 as determined by Y2H assays.

Supplemental Figure 5. Determination of the interaction of ARID5 and CHR11 with truncated versions of RLT2 by an in vitro pull-down assay.

Supplemental Figure 6. Morphological phenotypes of wild type, *arid5*, and *rlt1/2*.

Supplemental Figure 7. The diurnal expression patterns of *FLC*, *SVP*, *FT*, and *SEP3* in wild type, *arid5*, *rlt1/2*, and *chr11/17*.

Supplemental Figure 8. Gene-ontology analysis of DEGs co-regulated in *arid5*, *rlt1/2*, and *chr11/17*.

Supplemental Figure 9. The expression of *Myc*-tagged wild type and mutated *ARID5* transgenes as determined by immunoblotting.

Supplemental Figure 10. Complementation of the morphological abnormalities of the *arid5* mutant by *GFP*-tagged wild type and mutated *ARID5* transgenes.

Supplemental Figure 11. Structure and histone binding by the ARID5 PHD finger.

Supplemental Figure 12. Heatmaps showing the occupancy of ARID5 and H3K4me3 around the TSS.

Supplemental Figure 13. Browser view of the ChIP-seq signals of H3K4me3 and ARID5-GFP.

Supplemental Figure 14. Determination of the relationship between ARID5- or H3K4me3-enriched genes and DEGs co-regulated in the *arid5*, *rlt1/2*, and *chr11/17* mutants.

Supplemental Table 1. MS analyses of proteins co-purified with indicated bait proteins in corresponding transgenic plants.

Supplemental Table 2. List of protein–protein interactions as determined by Y2H.

Supplemental Table 3. Data collection and refinement statistics.

Supplemental Table 4. Identification of significantly enriched motifs in ARID5-bound chromatin regions by Homer de novo motif analysis.

Supplemental Data Set 1. Full list of co-purified proteins as determined by MS.

Supplemental Data Set 2. DEGs identified by RNA-seq.

Supplemental Data Set 3. ARID5 peaks identified by ChIP-seq.

Supplemental Data Set 4. DNA oligos used in the study.

ACKNOWLEDGMENTS

We thank the staff at beamline BL19U1 of the National Center for Protein Sciences Shanghai at the Shanghai Synchrotron Radiation Facility for the collection of x-ray data. This work was supported by the National Key Research and Development Program of China from the Chinese Ministry of Science and Technology (2016YFA0500801 to X.-J.H.), the National Natural Science Foundation of China (31770782), Special Support from SUSTech (G02226301), the Shenzhen Government Peacock Plan (Y01226143), and the National Key Laboratory of Plant Molecular Genetics (to J.D.).

AUTHOR CONTRIBUTIONS

L.-M.T., B.-W.G., C.-J.Z., J.G., C.-R.S., L.L., and S.C. performed the biological and biochemical experiments; R.L., J.L., Y.W., L.C., X.D., and S.L. performed the structural and biochemical experiments; Y.-N.S., R.-N.L., and X.-W.C. performed bioinformatics analyses; J.D. and X.-J.H. conceived the study, designed the experiments, and wrote the article.

Received December 9, 2019; revised April 9, 2020; accepted April 27, 2020; published April 30, 2020.

REFERENCES

Adams, P.D., et al. (2010). PHENIX: A comprehensive Python-based system for macromolecular structure solution. Acta Crystallogr. D Biol. Crystallogr. **66:** 213–221.

Amasino, R. (2010). Seasonal and developmental timing of flowering. Plant J. **61:** 1001–1013.

Bartholomew, B. (2014). ISWI chromatin remodeling: One primary actor or a coordinated effort? Curr. Opin. Struct. Biol. **24:** 150–155.

Bäurle, I., and Dean, C. (2006). The timing of developmental transitions in plants. Cell **125:** 655–664.

Berr, A., Shafiq, S., and Shen, W.H. (2011). Histone modifications in transcriptional activation during plant development. Biochim. Biophys. Acta **1809:** 567–576.

Bouché, F., Lobet, G., Tocquin, P., and Périlleux, C. (2016). FLORID: An interactive database of flowering-time gene networks in *Arabidopsis thaliana*. Nucleic Acids Res. **44** (D1): D1167–D1171.

Buels, R., Yao, E., Diesh, C.M., Hayes, R.D., Munoz-Torres, M., Helt, G., Goodstein, D.M., Elsik, C.G., Lewis, S.E., Stein, L., and Holmes, I.H. (2016). JBrowse: A dynamic web platform for genome visualization and analysis. Genome Biol. **17:** 66.

Cai, S., Zhu, L., Zhang, Z., and Chen, Y. (2007). Determination of the three-dimensional structure of the Mrf2-DNA complex using paramagnetic spin labeling. Biochemistry **46:** 4943–4950.

Chica, C., Szarzynska, B., Chen-Min-Tao, R., Duvernois-Berthet, E., Kassam, M., Colot, V., and Roudier, F. (2013). Profiling spatial enrichment of chromatin marks suggests an additional epigenomic dimension in gene regulation. Front. Life Sci. **7:** 80–87.

Clapier, C.R., and Cairns, B.R. (2009). The biology of chromatin remodeling complexes. Annu. Rev. Biochem. **78:** 273–304.

Cock, P.J., Fields, C.J., Goto, N., Heuer, M.L., and Rice, P.M. (2010). The Sanger FASTQ file format for sequences with quality scores, and the Solexa/Illumina FASTQ variants. Nucleic Acids Res. **38:** 1767–1771.

Cui, X., et al. (2016). REF6 recognizes a specific DNA sequence to demethylate H3K27me3 and regulate organ boundary formation in Arabidopsis. Nat. Genet. **48:** 694–699.

Dong, J., Gao, Z., Liu, S., Li, G., Yang, Z., Huang, H., and Xu, L. (2013). SLIDE, the protein interacting domain of Imitation Switch remodelers, binds DDT-domain proteins of different subfamilies in chromatin remodeling complexes. J. Integr. Plant Biol. **55:** 928–937.

Du, J., Johnson, L.M., Groth, M., Feng, S., Hale, C.J., Li, S., Vashisht, A.A., Wohlschlegel, J.A., Patel, D.J., and Jacobsen, S.E. (2014). Mechanism of DNA methylation-directed histone methylation by KRYPTONITE. Mol. Cell **55:** 495–504.

Du, J., et al. (2012). Dual binding of chromomethylase domains to H3K9me2-containing nucleosomes directs DNA methylation in plants. Cell **151:** 167–180.

Emsley, P., Lohkamp, B., Scott, W.G., and Cowtan, K. (2010). Features and development of Coot. Acta Crystallogr. D Biol. Crystallogr. **66:** 486–501.

Fleischer, T.C., Yun, U.J., and Ayer, D.E. (2003). Identification and characterization of three new components of the mSin3A corepressor complex. Mol. Cell. Biol. **23:** 3456–3467.

Gkikopoulos, T., Schofield, P., Singh, V., Pinskaya, M., Mellor, J., Smolle, M., Workman, J.L., Barton, G.J., and Owen-Hughes, T. (2011). A role for Snf2-related nucleosome-spacing enzymes in genome-wide nucleosome organization. Science **333:** 1758–1760.

Heinz, S., Benner, C., Spann, N., Bertolino, E., Lin, Y.C., Laslo, P., Cheng, J.X., Murre, C., Singh, H., and Glass, C.K. (2010). Simple combinations of lineage-determining transcription factors prime cis-regulatory elements required for macrophage and B cell identities. Mol. Cell **38:** 576–589.

Huanca-Mamani, W., Garcia-Aguilar, M., León-Martínez, G., Grossniklaus, U., and Vielle-Calzada, J.P. (2005). CHR11, a chromatin-remodeling factor essential for nuclear proliferation during female gametogenesis in *Arabidopsis thaliana*. Proc. Natl. Acad. Sci. USA **102:** 17231–17236.

Imaizumi, T., and Kay, S.A. (2006). Photoperiodic control of flowering: not only by coincidence. Trends Plant Sci. **11:** 550–558.

Iwahara, J., Iwahara, M., Daughdrill, G.W., Ford, J., and Clubb, R.T. (2002). The structure of the Dead ringer-DNA complex reveals how AT-rich interaction domains (ARIDs) recognize DNA. EMBO J. **21:** 1197–1209.

Jarillo, J.A., Piñeiro, M., Cubas, P., and Martínez-Zapater, J.M. (2009). Chromatin remodeling in plant development. Int. J. Dev. Biol. **53:** 1581–1596.

Kim, D., Langmead, B., and Salzberg, S.L. (2015). HISAT: A fast spliced aligner with low memory requirements. Nat. Methods **12:** 357–360.

Klose, R.J., Kallin, E.M., and Zhang, Y. (2006). JmjC-domain-containing proteins and histone demethylation. Nat. Rev. Genet. **7:** 715–727.

Langmead, B., and Salzberg, S.L. (2012). Fast gapped-read alignment with Bowtie 2. Nat. Methods **9:** 357–359.

Li, B., Carey, M., and Workman, J.L. (2007). The role of chromatin during transcription. Cell **128:** 707–719.

Li, C., et al. (2016a). Concerted genomic targeting of H3K27 demethylase REF6 and chromatin-remodeling ATPase BRM in Arabidopsis. Nat. Genet. **48:** 687–693.

Li, D., Liu, J., Liu, W., Li, G., Yang, Z., Qin, P., and Xu, L. (2017). The ISWI remodeler in plants: Protein complexes, biochemical functions, and developmental roles. Chromosoma **126:** 365–373.

Li, G., Liu, S., Wang, J., He, J., Huang, H., Zhang, Y., and Xu, L. (2014). ISWI proteins participate in the genome-wide nucleosome distribution in Arabidopsis. Plant J. **78:** 706–714.

Li, G., Zhang, J., Li, J., Yang, Z., Huang, H., and Xu, L. (2012). Imitation Switch chromatin remodeling factors and their interacting RINGLET proteins act together in controlling the plant vegetative phase in Arabidopsis. Plant J. **72:** 261–270.

Li, H., Ilin, S., Wang, W., Duncan, E.M., Wysocka, J., Allis, C.D., and Patel, D.J. (2006). Molecular basis for site-specific read-out of histone H3K4me3 by the BPTF PHD finger of NURF. Nature **442:** 91–95.

Li, S., Liu, L., Li, S., Gao, L., Zhao, Y., Kim, Y.J., and Chen, X. (2016b). SUVH1, a Su(var)3-9 family member, promotes the expression of genes targeted by DNA methylation. Nucleic Acids Res. **44:** 608–620.

Li, S., Yang, Z., Du, X., Liu, R., Wilkinson, A.W., Gozani, O., Jacobsen, S.E., Patel, D.J., and Du, J. (2016c). Structural basis for the unique multivalent readout of unmodified H3 tail by Arabidopsis ORC1b BAH-PHD cassette. Structure **24:** 486–494.

Li, X., Harris, C.J., Zhong, Z., Chen, W., Liu, R., Jia, B., Wang, Z., Li, S., Jacobsen, S.E., and Du, J. (2018). Mechanistic insights into plant SUVH family H3K9 methyltransferases and their binding to context-biased non-CG DNA methylation. Proc. Natl. Acad. Sci. USA **115:** E8793–E8802.

Li, Y., and Li, H. (2012). Many keys to push: Diversifying the 'readership' of plant homeodomain fingers. Acta Biochim. Biophys. Sin. (Shanghai) **44:** 28–39.

Liu, C., Xin, Y., Xu, L., Cai, Z., Xue, Y., Liu, Y., Xie, D., Liu, Y., and Qi, Y. (2018b). Arabidopsis ARGONAUTE 1 binds chromatin to promote gene transcription in response to hormones and stresses. Dev. Cell **44:** 348–361.e7.

Liu, R., Li, X., Chen, W., and Du, J. (2018a). Structure and mechanism of plant histone mark readers. Sci. China Life Sci. **61:** 170–177.

Martínez-Balbás, M.A., Tsukiyama, T., Gdula, D., and Wu, C. (1998). Drosophila NURF-55, a WD repeat protein involved in histone metabolism. Proc. Natl. Acad. Sci. USA **95:** 132–137.

Mashtalir, N., et al. (2018). Modular organization and assembly of SWI/SNF family chromatin remodeling complexes. Cell **175:** 1272–1288.e20.

Murshudov, G.N., Vagin, A.A., and Dodson, E.J. (1997). Refinement of macromolecular structures by the maximum-likelihood method. Acta Crystallogr. D Biol. Crystallogr. **53:** 240–255.

Narlikar, G.J. (2010). A proposal for kinetic proof reading by ISWI family chromatin remodeling motors. Curr. Opin. Chem. Biol. **14:** 660–665.

Ning, Y.Q., Ma, Z.Y., Huang, H.W., Mo, H., Zhao, T.T., Li, L., Cai, T., Chen, S., Ma, L., and He, X.J. (2015). Two novel NAC transcription factors regulate gene expression and flowering time by associating with the histone demethylase JMJ14. Nucleic Acids Res. **43:** 1469–1484.

O'Malley, R.C., Huang, S.C., Song, L., Lewsey, M.G., Bartlett, A., Nery, J.R., Galli, M., Gallavotti, A., and Ecker, J.R. (2016). Cistrome and epicistrome features shape the regulatory DNA landscape. Cell **165:** 1280–1292.

Otwinowski, Z., and Minor, W. (1997). Processing of x-ray diffraction data collected in oscillation mode. Methods Enzymol. **276:** 307–326.

Patel, D.J. (2016). A structural perspective on readout of epigenetic histone and DNA methylation marks. Cold Spring Harb. Perspect. Biol. **8:** a018754.

Rajakumara, E., Law, J.A., Simanshu, D.K., Voigt, P., Johnson, L.M., Reinberg, D., Patel, D.J., and Jacobsen, S.E. (2011). A dual flip-out mechanism for 5mC recognition by the Arabidopsis SUVH5 SRA domain and its impact on DNA methylation and H3K9 dimethylation in vivo. Genes Dev. **25:** 137–152.

Ramírez, F., Dündar, F., Diehl, S., Grüning, B.A., and Manke, T. (2014). deepTools: A flexible platform for exploring deep-sequencing data. Nucleic Acids Res. **42:** W187–W191.

Ruthenburg, A.J., Li, H., Milne, T.A., Dewell, S., McGinty, R.K., Yuen, M., Ueberheide, B., Dou, Y., Muir, T.W., Patel, D.J., and Allis, C.D. (2011). Recognition of a mononucleosomal histone modification pattern by BPTF via multivalent interactions. Cell **145:** 692–706.

Shen, L., Shao, N., Liu, X., and Nestler, E. (2014). ngs.plot: Quick mining and visualization of next-generation sequencing data by integrating genomic databases. BMC Genomics **15:** 284.

Smaczniak, C., et al. (2012). Characterization of MADS-domain transcription factor complexes in Arabidopsis flower development. Proc. Natl. Acad. Sci. USA **109:** 1560–1565.

Stroud, H., Do, T., Du, J., Zhong, X., Feng, S., Johnson, L., Patel, D.J., and Jacobsen, S.E. (2014). Non-CG methylation patterns shape the epigenetic landscape in Arabidopsis. Nat. Struct. Mol. Biol. **21:** 64–72.

Sun, X., Feng, P., Xu, X., Guo, H., Ma, J., Chi, W., Lin, R., Lu, C., and Zhang, L. (2011). A chloroplast envelope-bound PHD transcription factor mediates chloroplast signals to the nucleus. Nat. Commun. **2:** 477.

Toto, M., D'Angelo, G., and Corona, D.F. (2014). Regulation of ISWI chromatin remodelling activity. Chromosoma **123:** 91–102.

Wang, L., Feng, Z., Wang, X., Wang, X., and Zhang, X. (2010). DEGseq: An R package for identifying differentially expressed genes from RNA-seq data. Bioinformatics **26:** 136–138.

Wilsker, D., Patsialou, A., Dallas, P.B., and Moran, E. (2002). ARID proteins: A diverse family of DNA binding proteins implicated in the control of cell growth, differentiation, and development. Cell Growth Differ. **13:** 95–106.

Wysocka, J., Swigut, T., Xiao, H., Milne, T.A., Kwon, S.Y., Landry, J., Kauer, M., Tackett, A.J., Chait, B.T., Badenhorst, P., Wu, C., and Allis, C.D. (2006). A PHD finger of NURF couples histone H3 lysine 4 trimethylation with chromatin remodelling. Nature **442:** 86–90.

Xiao, H., Sandaltzopoulos, R., Wang, H.M., Hamiche, A., Ranallo, R., Lee, K.M., Fu, D., and Wu, C. (2001). Dual functions of largest NURF subunit NURF301 in nucleosome sliding and transcription factor interactions. Mol. Cell **8:** 531–543.

Yadon, A.N., and Tsukiyama, T. (2011). SnapShot: Chromatin remodeling: ISWI. Cell **144:** 453–453.e1.

Zhang, C.J., Zhou, J.X., Liu, J., Ma, Z.Y., Zhang, S.W., Dou, K., Huang, H.W., Cai, T., Liu, R., Zhu, J.K., and He, X.J. (2013). The splicing machinery promotes RNA-directed DNA methylation and transcriptional silencing in Arabidopsis. EMBO J. **32:** 1128–1140.

Zhang, S., et al. (2015). C-terminal domains of a histone demethylase interact with a pair of transcription factors and mediate specific chromatin association. Cell Discov. **1:** 15003.

Zhang, Y., Liu, T., Meyer, C.A., Eeckhoute, J., Johnson, D.S., Bernstein, B.E., Nusbaum, C., Myers, R.M., Brown, M., Li, W., and Liu, X.S. (2008). Model-based analysis of ChIP-seq (MACS). Genome Biol. **9:** R137.

Zhu, H., Chen, T., Zhu, M., Fang, Q., Kang, H., Hong, Z., and Zhang, Z. (2008). A novel ARID DNA-binding protein interacts with SymRK and is expressed during early nodule development in *Lotus japonicus*. Plant Physiol. **148:** 337–347.